

DARE2X

Decentralised Ammonia production from Renewable Energy utilising novel sorption-enhanced plasma-catalytic Power-to-X technology

D4.2 - Summary of experiments WP4 (methods, results, data)

University of Liverpool

DATE: 31/03/2025

Abstract: Ammonia synthesis via plasma-catalytic methods was investigated to overcome the limitations of the energy-intensive Haber-Bosch process. A zero-dimensional plasma kinetics model was developed and validated, showing good agreement with experimental data. Experimental results demonstrated the critical role of catalyst support and metal loading. Multiple support materials were tested, and the best catalyst were made with zeolites. This deliverable summarises the work of WP4.

PROJECT DATA	
Project Acronym	DARE2X
Project Title	Decentralised Ammonia production from Renewable Energy utilising novel sorption-enhanced plasma-catalytic Power-to-X technology
Project number	101083905
Call identifier	HORIZON-CL5-2021-D3-03
Topic identifier	HORIZON-CL5-2021-D3-03-02 Next generation of renewable energy technologies
Type of action	Research and Innovation Actions
Project Duration	36 months (From 1 st October 2022)
Coordinator	Teknologisk Institut (DTI), Denmark - Christoffer Mølleskov Pedersen chm@teknologisk.dk
Website	www.dare2x.eu
DELIVERABLE DOCUMENT SHEET	
Deliverable No.	4.2
Deliverable title	Summary of experiments WP4 (methods, results, data)
Description	Summary of work performed in WP4
WP No.	WP4
Related task	T4.1 – T4.4
Lead Beneficiary	University of Liverpool
Author(s)	
Contributor(s)	
Type ¹	Report (R)
Dissemination Level ²	Public
Language	English – GB

¹ R: Document, report; DEM: Demonstrator, pilot, prototype; DEC: Website, video etc., DATA: Data sets; DMP: Data management plan; ETHICS; SECURITY; Other: Software, technical diagram, algorithms, models etc.

² PU: Public, fully open; SEN: Sensitive.

Deliverable 4.2 Summary of experiments WP4 (methods, results, data)

University of Liverpool

31st March 2025

1. Introduction

Ammonia synthesis plays a crucial role in various industrial processes, particularly in the production of fertilizers, which are essential for global food production. The traditional Haber-Bosch method for ammonia synthesis is energy-intensive, requiring high temperatures and pressures, leading to significant energy consumption and greenhouse gas emissions [1-3]. In response to these challenges, plasma-catalytic ammonia synthesis has emerged as a promising alternative, offering the potential for more energy-efficient and environmentally friendly production. This method involves the use of non-thermal plasma to activate nitrogen and hydrogen molecules, with the assistance of catalysts to facilitate ammonia formation at lower temperatures and pressures [4-6].

Catalysts are key to improving the efficiency and selectivity of plasma-catalytic processes, and their performance can be influenced by the choice of support material and metal catalysts. Various catalyst supports, such as transition metal-loaded supports and zeolite-based materials [7-14], have been explored in plasma-assisted ammonia synthesis due to their unique properties, including high surface area, tunable acidity, and thermal stability. These supports help disperse active metal sites, enhance electron transfer, and promote the interaction with plasma, all of which contribute to improved ammonia yields.

This project investigates the role of various catalyst supports, including γ -Al₂O₃, carbon black, MgO, and zeolites, in plasma-catalytic ammonia synthesis. It examines transition metals (Ni, Co, Fe) and precious metals (Pt, Ru) as active components, along with Ba and Ca as promoters to enhance catalytic performance. By analyzing catalyst behavior under different plasma conditions, the study aims to optimize metal-support interactions for improved ammonia yield and energy efficiency. Additionally, it explores the impact of metal-loading techniques on catalyst stability and long-term

performance. Specifically, WP4 is dedicated to developing and evaluating innovative catalyst designs aimed at improving plasma-catalytic ammonia production and enhancing energy efficiency.

Despite rigorous experimental investigations, a comprehensive understanding of the underlying plasma mechanisms has not yet been fully characterized due to the complex nature of the discharge environment. Therefore, a thorough understanding of plasma chemistry in DBD plasma-assisted ammonia synthesis is critical for achieving high energy efficiency and a high ammonia synthesis rate, both of which are essential for the successful scale-up and application of this technology.

In this deliverable 4.3, our research is also dedicated to gaining a fundamental understanding of plasma chemistry and formation pathways in plasma-assisted ammonia synthesis. To achieve this, we performed computational plasma chemical kinetics modeling to elucidate the possible chemical pathways for plasma-assisted ammonia synthesis.

2. Methods

2.1 Numerical method and kinetic model

A zero-dimensional (0D) plasma kinetic model, incorporating various atoms, radicals, excited species, neutral molecules, and ions, is developed to obtain insights into the underlying mechanism of plasma-assisted ammonia synthesis processes. The plasma kinetics solver ZDPlasKin, which integrates the Boltzmann equation solver BOLSIG+, is employed to determine the time evolution of species densities generated in the reaction chamber [8]. A schematic diagram illustrating the execution flow of ZDPlasKin is presented in Figure 1. It solves the continuity equations for species densities, as described in Equation 1:

$$\frac{dn_i}{dt} = \sum_j \left[(a_{ij}^R - a_{ij}^L) k_j \prod_l n_l \right] \quad (\text{Eq.1})$$

where n_i stands for the density of species i , a_{ij}^R and a_{ij}^L are the stoichiometric coefficients of species i on the right- and left- hand sides of reaction j , respectively. n_l is the density of species l on the left side of the reaction j , and k_j is the rate coefficient of reaction j .

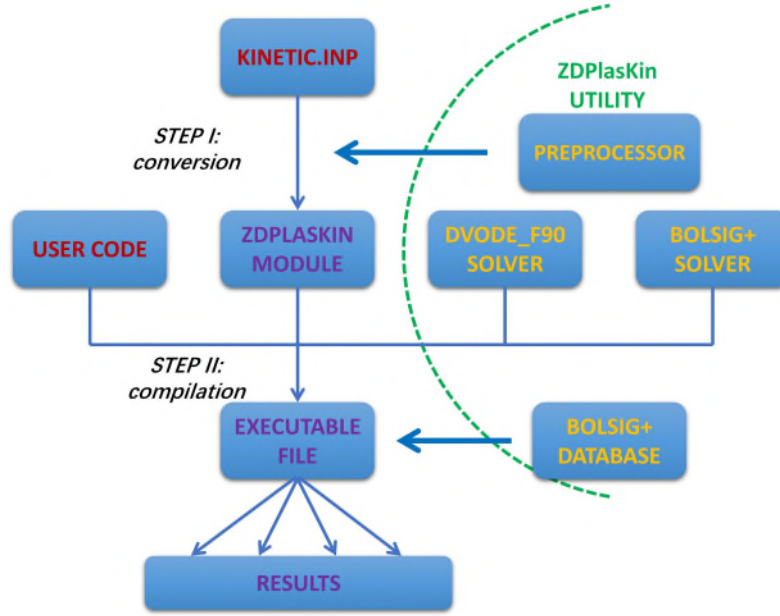


Figure 1. Schematic diagram of the execution flow of ZDPlasKin.

The electric field E , at which BOLSIG+ solves the Boltzmann equation, is calculated using the differential form of the Joule heating equation [9], shown in Equation 2, as:

$$\frac{dP}{dV} = JE = \sigma E^2 \quad (\text{Eq.2})$$

where P is the power, dV is a volume element, J is the current density, and σ is the electron conductivity. Assuming no spatial dependence, the reduced electric field (E/N) thus can be calculated from the power density $p = P/V$ by the Equation 3:

$$\left(\frac{E}{N}\right) = \frac{1}{N} \sqrt{\frac{p}{\sigma}} \quad (\text{Eq.3})$$

where N is the total number density of gas-phase species. The electron conductivity is calculated by the Equation 4:

$$\sigma = en_e \mu_e \quad (\text{Eq.4})$$

where e is the elementary charge, n_e is the electron number density, and μ_e is the electron mobility, calculated by BOLSIG+ [10]. This reduced electric field is calculated at each time step due to the changing gas composition as a function of time.

2.2 Kinetic Mechanism of Plasma

In this work, we propose a detailed kinetic mechanism for DBD plasma-assisted

ammonia synthesis, which includes electron impact reactions, neutral-neutral and neutral-ion reactions, electron-ion recombination, and reactions involving excited species. The rate coefficients for electron impact reactions are calculated using BOLSIG+ by solving the Boltzmann equation based on electron impact cross sections data. Most of these cross sections are available in the online LXCat database (<https://nl.lxcat.net>). The cross sections for the ionization and dissociative ionization of NH₃ molecule are obtained from Itikawa's work [11]. The gas-phase chemistry set is primarily built upon Sun's work [12], with additional reactions integrated from the NIST Chemical Kinetics Database (<https://kinetics.nist.gov/kinetics>).

Furthermore, the plasma kinetic model incorporates a detailed description of vibrational kinetics, including vibrational-translational (V-T) relaxation, vibrational-vibrational (V-V) energy exchange between two same molecules and V-V' interactions among two different molecules as well as chemical reactions accelerated by vibrationally excited molecules. The rate coefficients for V-T and V-V relaxations are determined using the Schwartz-Slowsky-Herzfeld (SSH) theory [13,14]. Meanwhile, the rate coefficient for chemical reactions involving vibrational species can be calculated by the theoretical-information approach, as given in Eq.5

$$k_R(E_v, T_0) = k_{R0} \exp\left(-\frac{E_a - \alpha E_v}{T_0}\right) \theta(E_a - \alpha E_v) \quad (\text{Eq.5})$$

here, k_{R0} is the pre-exponential factor, T_0 is the translational gas temperature, E_a is the activation energy barrier for the chemical reaction, E_v is the vibrational energy of a vibrationally-excited molecule, and $\theta(x)$ is the Heaviside step function ($\theta(x) = 1$ when $x \geq 0$; and $\theta(x) = 0$ when $x < 0$). The coefficient α for the efficiency of vibrational energy can be calculated based on the Fridman-Mecheret α -model [15].

$$\alpha = \frac{E_a^f}{E_a^f + E_a^b} \quad (\text{Eq.6})$$

The superscript f and b stand for forward and backward reactions.

To describe the electronic kinetics, the model incorporates a set of reactions, including electronic transitions between N₂(A3) and N₂(B3) mediated by N₂(v), optical transitions, and interactions of electronically excited species through collisions with

electronic states and neutral species. The reactions describing electronic states of N and N₂ are adopted from Sun *et al* [12]. Furthermore, ion-neutral reactions, electron-ion recombination reactions, and neutralization reactions are all accounted for in the ion chemistry mechanism. The kinetic parameters for these processes are obtained from the UMIST Database for Astrochemistry (<https://udfa.ajmarkwick.net>). As a result, the model considers 41 species and 520 elementary reactions for the plasma assisted ammonia synthesis process. A complete list of species included in this model is provided in Table 1.

Table 1. Species considered in the numerical modelling.

Species type	Symbol	Number
Molecules	N ₂ , H ₂ , NH ₃	3
Atoms/radicals	H, N, NH, NH ₂	4
Vibrational states	H ₂ (v1), H ₂ (v2), H ₂ (v3), N ₂ (v1), N ₂ (v2), N ₂ (v3), N ₂ (v4), N ₂ (v5), N ₂ (v6), N ₂ (v7), N ₂ (v8), NH ₃ (v2), NH ₃ (v4), NH ₃ (v13)	14
Electronic states	N ₂ (A3), N ₂ (B3), N ₂ (a'1), N ₂ (C3), N(² D), N(² P)	6
Ions	H ⁺ , H ₂ ⁺ , H ₃ ⁺ , N ⁺ , N ₂ ⁺ , N ₃ ⁺ , N ₄ ⁺ , NH ⁺ , NH ₂ ⁺ , NH ₃ ⁺ , NH ₄ ⁺ , N ₂ H ⁺ , H ⁻ , e	14

Note: N₂(A3) is the sum of N₂(A³Σ_u⁺, v=0-4), N₂(A³Σ_u⁺, v=5-9), and N₂(A³Σ_u⁺, v=10); N₂(B3) is the sum of N₂(B³Π_g), N₂(W³Δ_u), and N₂(B'³Σ_u⁻); N₂(a'1) is the sum of N₂(a'¹Σ_u⁻), N₂(a¹Π_g), and N₂(w¹Δ_u); N₂(C3) is the sum of N₂(C³Π_u), N₂(E³Σ_g⁺), and N₂(a''¹Σ_g⁺).

2.3 Discharge description in the model

In reality, an AC-activated DBD plasma typically exhibits a filamentary character, consisting of micro-discharge filaments and weaker plasma in between [16]. To mimic

the conditions of AC-activated DBD plasmas, we defined time-dependent periodically pulsed power density functions. The power density in between those pulses (i.e., micro-discharges) was nonzero and significantly influenced the outcome of the calculations. Power density profiles were used, mimicking both filamentary and more uniform DBDs, to determine gas phase compositions of radicals in actual plasma conditions [9]. Both the micro-discharges (strong plasma) and their afterglows (weak plasma) in a filamentary plasma are considered. Those conditions correspond to a maximum power density of 7.65×10^6 W/cm³ and to a minimum power density of 1.25 W/cm³, respectively. The gas temperature in the discharge region was measured using a fiber optical thermometer (Omega, FOB102).

2.4 Materials

The synthesis and sourcing of catalysts for this study were carried out through a collaborative effort. The γ -Al₂O₃, carbon black, MgO, mordenite, and Y-zeolite-based catalysts were synthesized by DTI, ensuring controlled preparation methods and consistency in material properties. Meanwhile, all ultra-stable Y (USY)-based catalysts were synthesized by Katja from the National Institute of Chemistry (NIC). Additionally, Zeolite I, II, III, and IV were obtained from Fluka Chemie GmbH and their modification was performed by Xin Tu's group.

2.4.1 Preparation of Metal/Zeolite Catalysts via the Incipient Wetness Impregnation Method

All chemicals used in this study were sourced from Fisher Scientific. The metal-loaded zeolite catalysts were prepared using the incipient wetness impregnation method, also known as the dry impregnation method. This process involves dissolving the desired metal precursor in a liquid solvent, such as distilled water, to create a homogeneous solution. The zeolite support, in powder form, is then added to the solution, forming a slurry that is stirred for 30 minutes at room temperature to ensure uniform dispersion of the metal precursor.

Following this, the impregnation step takes place over 12 hours at room temperature, during which capillary action facilitates the absorption of the metal-containing solution into the pores of the zeolite support. After impregnation, the mixture

undergoes drying in an oven at 110 °C for 12 hours to remove excess solvent, followed by calcination in a muffle furnace at 500 °C for 4 hours, with a controlled heating rate of 5 °C min⁻¹. This calcination step decomposes the metal precursor, leading to the formation of metal oxide species on the zeolite support.

Finally, the metal oxide/zeolite composite is subjected to a reduction process in a hydrogen atmosphere (30% H₂ in Ar) at a specific temperature for 5 hours. This reduction step converts the metal oxides into their active metallic forms, yielding the final metal/zeolite catalyst for further characterization and catalytic testing.

2.4.2 Preparation of Metal-Zeolite Catalysts via Ion-Exchange Method

Metal-zeolites were synthesized using the ion-exchange method. Initially, a specified amount of metal nitrate was dissolved in 50 mL of distilled water to prepare a 0.1 M metal nitrate solution. To this solution, 2 g of zeolite 5A support was added, and the mixture was stirred using a magnetic stirrer for 12 hours. During this time, metal ions from the solution exchanged with the cations in the zeolite structure.

Following the ion-exchange process, the zeolite was washed by centrifugation at 6000 rpm for 5 cycles, using distilled water to remove any unexchanged metal ions. The washed zeolite was then dried in an oven at 110 °C. Subsequently, the dried zeolite was calcined in a muffle furnace at 500 °C for 4 hours, with a controlled temperature ramp of 5 °C min⁻¹, resulting in the formation of metal oxide-zeolite composites.

Finally, the metal oxide-zeolite catalysts were reduced in a hydrogen atmosphere (30% H₂ in Ar) at a specific temperature for 5 hours, converting the metal oxides into their active metallic forms, and yielding the final metal-zeolite catalyst.

2.5 Experimental setup

Plasma-catalytic ammonia production experiments were conducted in a coaxial dielectric barrier discharge (DBD) reactor, as detailed in Deliverable D4.1. The schematic of the system is shown in Figure 2. A 4 mm inner diameter, 1 mm thick quartz tube acted as the dielectric, while a 20 mm long stainless-steel mesh wire wrapped around it served as the ground electrode. A 2 mm diameter stainless-steel rod inserted into the quartz tube acted as the high-voltage electrode, creating a 1 mm discharge gap

between the quartz tube and the high-voltage electrode.

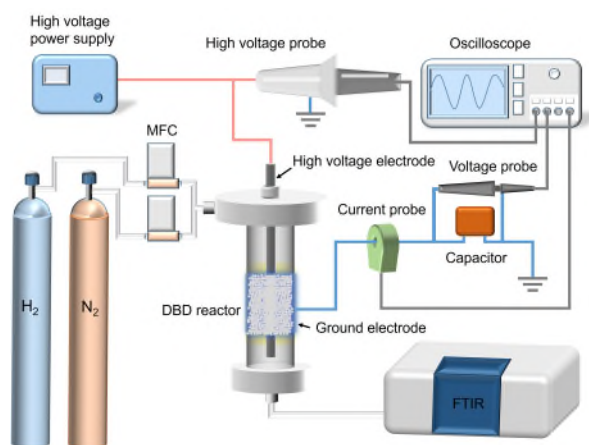


Figure 2. Schematic diagram of the plasma-catalytic ammonia production system.

An AC high-voltage power supply, delivering a peak-to-peak voltage of 30 kV at a frequency of 11 kHz, was used to generate plasma within the discharge gap. The voltage was monitored using a high-voltage probe (Tektronix P6015A), while the external capacitor voltage was measured with a voltage probe (Tektronix TPP0101), and the current was measured using a current monitor (Pearson 2877). All electrical signals were recorded on a four-channel digital oscilloscope (Tektronix MDO 3024). Power consumption was calculated via the Q-U Lissajous method. A catalyst load of 120 mg was placed within the discharge gap, and a mixture of pure N₂ and H₂ was fed into the system at a total flow rate of 40 mL min⁻¹, with an N₂/H₂ ratio of 1:3, unless otherwise stated. Ammonia concentration was measured using a Fourier Transform Infrared (FTIR, Jasco FT/IR-4200). Energy yield (E) for ammonia production was calculated as follows:

$$E \text{ (g kWh}^{-1}\text{)} = \frac{\text{Ammonia concentration (ppm)} \times \text{Flow rate (L/s)} \times 60 \times 60 \times 17}{\text{Discharge powder (kW)} \times 24.5 \text{ (L mol}^{-1}\text{)} \times 1000000} \quad (\text{Eq. 7})$$

3. Results and discussion

3.1 Validation of the model

As shown in Figure 3, model validation is performed by comparing the steady-state experimental results with the predicted values of NH₃ concentrations under identical conditions. As shown in Figure 3, ammonia concentration exhibits a clear upward trend with increasing input power, attributed to more energy deposited into the

discharge mixture. The model demonstrates good agreement with experimental data, achieving an accuracy of better than 10% for most cases (4 W, 8 W, and 12 W). However, a noticeable overestimation is observed for the predicted ammonia concentration at 16 W, where the maximum deviation reaches approximately 15%. Overall, some discrepancies exist between the calculated and measured ammonia concentrations. However, these differences are not unexpected in view of the large number of chemical reactions that can occur and the fact that the rate coefficients of several of these reactions are subject to large uncertainties. Nevertheless, we deliberately choose not to “tune” our model to reach a better agreement with the experiments without a real scientific basis. All assumptions in our model are grounded in logical and plausible physics. In conclusion, we believe that our model is sufficiently realistic to capture the underlying plasma chemistry in the DBD-assisted ammonia synthesis process.

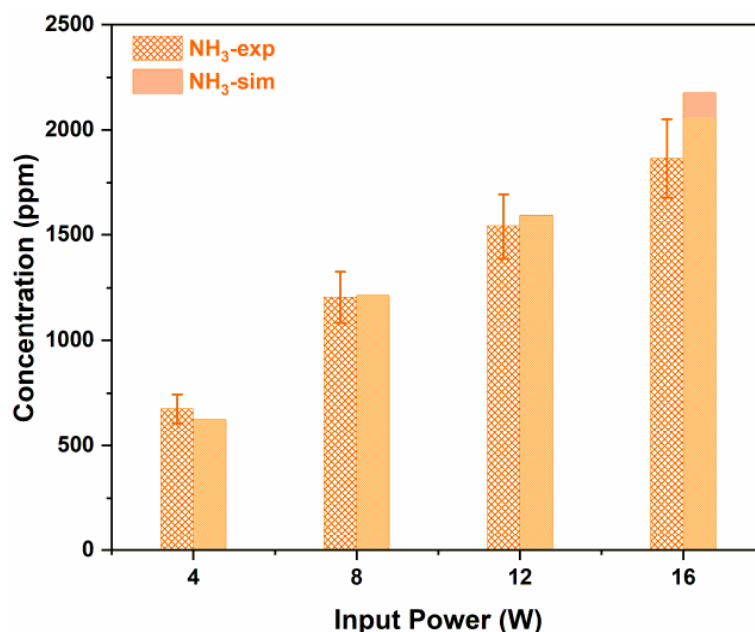


Figure 3. Comparison of NH₃ concentrations between steady-state measurements and model predictions as a function of input power in plasma assisted ammonia synthesis (error bar: 10%).

3.2 Chemical reaction pathway analysis

In this section, the underlying plasma chemistry mechanisms for ammonia synthesis in the DBD will be discussed. Indeed, a better insight into the dominant chemical reactions might help steer the process to improve ammonia synthesis.

The reduced electric field (i.e., the ratio of the electric field over total gas number

density, E/N) is one of the important parameters in controlling the direction of electron energy deposition and formation of active species in plasma discharge. Figure 4(a) shows the fractions of plasma energy deposited into different channels as a function of E/N in a 0.5 N₂/0.5 H₂ mixture discharge. The blue area indicates the range of E/N values for the discharge conditions solved in our kinetic model. The rotational excitation and vibrational excitation mode of H₂ dominate the plasma discharge at a relatively low reduced electric field (< 10 Td). When E/N values range from 10 Td to 30 Td, the majority of electron energy is allocated to the vibrational excitation of N₂. In our studied E/N range of 30-230 Td, as shown in Figure 4(b), the primary mechanism of energy loss shifts to H₂ dissociation and vibrational excitation of N₂. In this range, the electron impact dissociation of H₂ gradually becomes important with increasing E/N value. At high E/N values (> 230 Td), the primary mechanism remains H₂ dissociation.

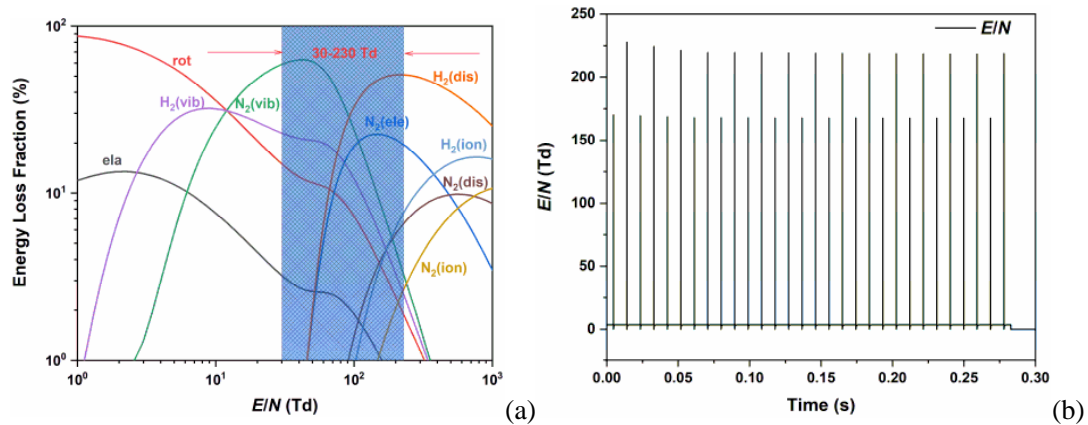


Figure 4. (a) Fractions of plasma energy deposited into different excitation modes in a 0.25 N₂/0.75 H₂ mixture as a function of E/N ; (b) time-resolved E/N (ela: elastic; rot: rotational excitation; vib: vibrational excitation; ele: electronic excitation; dis: dissociation; ion: ionization)

The time evolution of the number density for the most important species is presented in Figure 5. Generally, we see that the micro-discharges, because of their ns time scale, cause a pulsed behavior in atom and radical densities, with pulse widths on the ms scale. During micro-discharges, the electron density increases rapidly due to the ionization of both N₂ and H₂. N and N(²D) are initially formed via the electron impact reaction. In addition to the electron impact dissociation of N₂, the dissociation of N₂(A₃) also plays a significant role in atomic N formation. As a result, the number density of

N is higher than that of $N(^2D)$. Subsequently, N and $N(^2D)$ undergo successive hydrogenation, leading to the formation of NH and NH_2 radical. The concentration of NH_3 increases as the process propagates, primarily due to the recombination reactions $NH_2 + H + M \rightarrow NH_3 + M$ and $NH + H_2 + M \rightarrow NH_3 + M$. However, within the uniform plasma between micro-discharges, a decrease in the NH_3 profile is observed. This decline is attributed to the dissociation of NH_3 induced by electronically excited species $N_2(A3)$ and $N(^2D)$ (see figure 6), which coincides with an increase in NH_2 number density.

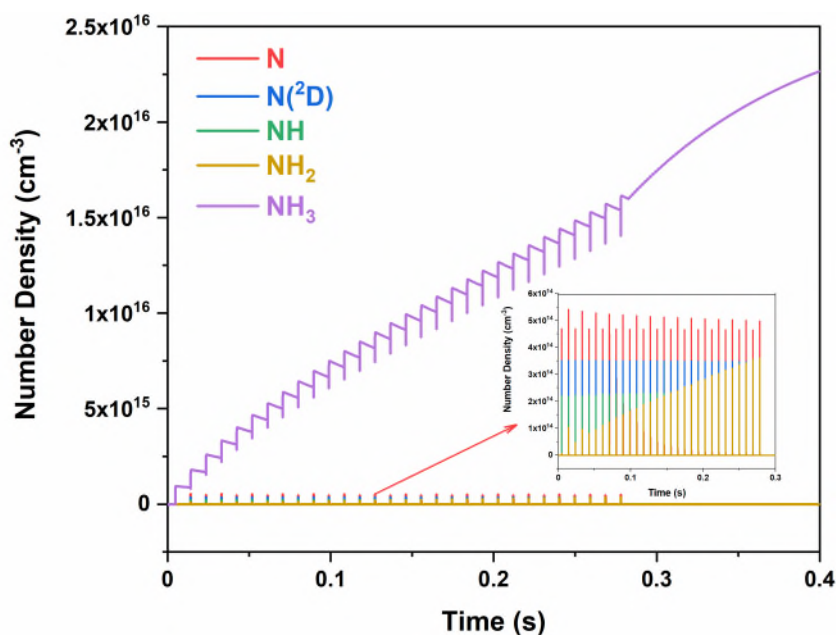


Figure 5. Time-dependent evolution of main species at an input power of 8 W, a gas flow rate of 40 mL min⁻¹.

To elucidate the underlying mechanism of ammonia formation, we present the reaction pathway analysis for plasma-assisted ammonia synthesis at a 40 mL min⁻¹ flow rate and 8 W input power in Figure 6. The thickest arrows represent the contribution of reactions to the species formation or consumption in the order of 10⁻⁶ mol cm⁻³, while the thinnest arrows represent the contribution of reactions in the order of 10⁻¹⁰ mol cm⁻³. The number attached to the arrows indicates the percentage of its relative contribution rate.

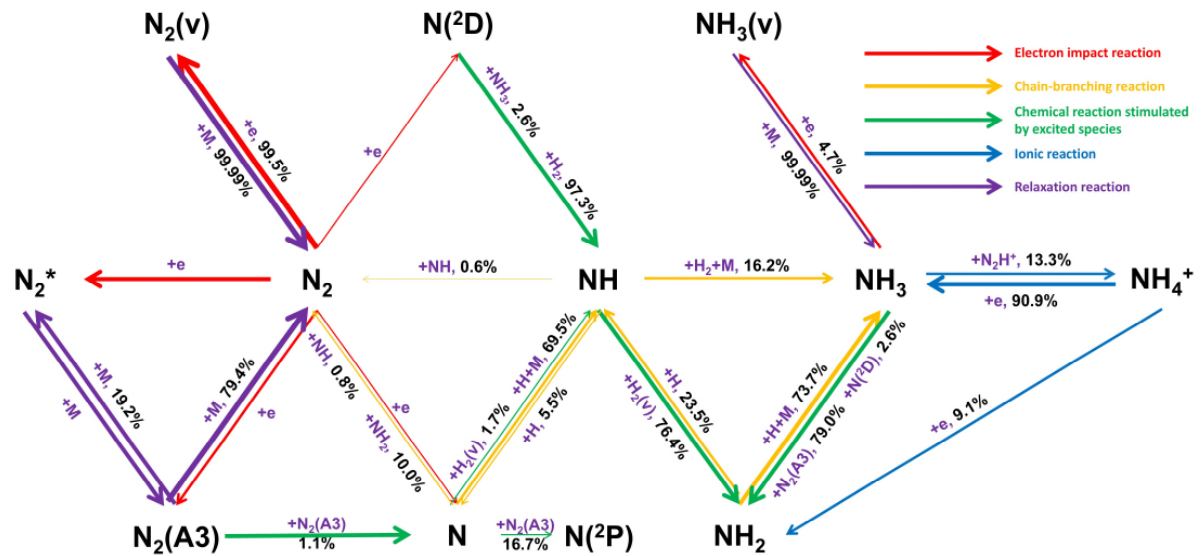


Figure 6. Network of ammonia formation pathways for plasma assisted N_2/H_2 conversion with a detailed chemistry set at an input power of 8 W (N_2^* includes $N_2(B3)$, $N_2(C3)$, and $N_2(a'1)$).

A significant portion of N_2 is consumed through electron impact excitation, $e + N_2 \rightarrow e + N_2(v)$, leading to the formation of vibrationally excited $N_2(v)$. More than 99.9% of $N_2(v)$ undergoes quenching to form the ground state N_2 , which contributes to a temperature rise in the N_2/H_2 mixture. Only a small part of N_2 is dissociated by electrons to produce N and $N(2D)$ and excited by electrons to generate electronically excited $N_2(A3)$. The results show that 1.1% of $N_2(A3)$ are consumed via the reaction $N_2(A3) + N_2(A3) \rightarrow N_2 + N + N$ to generate N atom, which serves as the primary pathway for atomic N formation. Among the N atoms produced, 0.8%, 10.0% recombine with NH and NH_2 radicals, respectively, via the reactions $N + NH \rightarrow N_2 + H$ and $N + NH_2 \rightarrow N_2 + H_2/2H$, leading to the regeneration of N_2 . Additionally, 16.7% of N atoms are excited by $N_2(A3)$ to form $N(2P)$ through the reaction $N + N_2(A3) \rightarrow N(2P) + N_2$. Beyond these two consumption pathways, the three-body reaction $N + H + M \rightarrow NH + M$ significantly contributes to N consumption, accounting for 69.5% of total N depletion. Furthermore, chain-branching reactions stimulated by excited $N(2D)$, particularly $N(2D) + H_2 \rightarrow NH + H$ and $N(2D) + NH_3 \rightarrow NH + NH_2$, are the key pathways for NH radical formation. It is noteworthy that vibrationally excited hydrogen, $H_2(v)$, accelerates NH consumption through the reaction $NH + H_2(v) \rightarrow NH_2 + H$ to form NH_2 , which accounts for 76.4% of total NH consumption. Additionally, 16.2% of NH radicals are consumed

through the recombination reaction $\text{NH} + \text{H}_2 + \text{M} \rightarrow \text{NH}_3 + \text{M}$, while it accounts for 8.0% of NH_3 formation. NH_2 primarily combines with H atom to form NH_3 , which is responsible for 73.7% of total NH_2 consumption. From the perspective of NH_3 formation, the reaction $\text{NH}_2 + \text{H} + \text{M} \rightarrow \text{NH}_3 + \text{M}$ is the dominant pathway, contributing 43.4% to total NH_3 production. Meanwhile, the dehydrogenation of NH_2 to NH accounts for 23.5% of total NH_2 consumption. Regarding NH_3 consumption, the primary pathway involves its dissociation by $\text{N}_2(\text{A}3)$ and $\text{N}(^2\text{D})$ to produce NH_2 radicals. The transformation of NH_3 to $\text{NH}_3(\text{v})$ via electron impact vibrational excitation ($\text{e} + \text{NH}_3 \rightarrow \text{e} + \text{NH}_3(\text{v})$) contributes to 4.7% of total NH_3 consumption. Furthermore, the ionic reaction $\text{NH}_3 + \text{N}_2\text{H}^+ \rightarrow \text{NH}_4^+ + \text{N}_2$ accounts for 13.3% of total NH_3 consumption. The NH_4^+ ion primarily recombines with electron to regenerate NH_3 . Furthermore, 9.1% of NH_4^+ undergoes recombination with electron to form NH_2 radicals.

3.3 Plasma-catalytic ammonia production from non-zeolite-based catalysts

3.3.1 Performance of transitional metals loaded catalysts

$\gamma\text{-Al}_2\text{O}_3$, carbon black, and MgO were evaluated as catalyst supports for plasma-catalytic ammonia synthesis, with transition metals acting as the active sites. Each support material offers distinct advantages and challenges that influence catalytic activity in different ways.

$\gamma\text{-Al}_2\text{O}_3$ has a high surface area, which enables better dispersion of active metal sites, enhancing their accessibility and improving reaction efficiency. Additionally, $\gamma\text{-Al}_2\text{O}_3$ is chemically stable under plasma conditions, which helps prevent unwanted side reactions and degradation over time. Compared to other support materials, $\gamma\text{-Al}_2\text{O}_3$ is cost-effective, widely available, and easily processed into various morphologies, making it a highly practical choice for catalyst development in plasma-catalytic systems.

Carbon black serves as an electrically conductive support, offering a unique set of advantages and challenges. Its conductivity enhances charge transfer and plasma-induced reactions, which may facilitate the electron-driven activation of N_2 and H_2 . Furthermore, its ability to interact effectively with plasma can generate stronger local

electric fields, potentially fostering radical formation. However, the impact of carbon black on ammonia synthesis remains less clear compared to oxide supports like $\gamma\text{-Al}_2\text{O}_3$ and MgO, necessitating further investigation.

MgO is another promising support due to its inherent basicity, thermal stability, and potential to enhance nitrogen activation. The basic sites on MgO may play a crucial role in adsorbing and activating nitrogen species, which is key to improving the efficiency of plasma-catalytic ammonia synthesis.

Effect of support, metal type, and loading:

Figure 7 illustrates the performance of catalysts supported on these materials. Both $\gamma\text{-Al}_2\text{O}_3$ and MgO-based catalysts exhibited a 2-3-fold enhancement in ammonia production compared to plasma-only conditions. In contrast, carbon black-based catalysts showed minimal to no improvement, regardless of the transition metal used. Among the metals tested, Ni and Co demonstrated higher catalytic activity than Cu, with Ni exhibiting the best overall performance. For Ni-loaded $\gamma\text{-Al}_2\text{O}_3$, increasing the metal loading had little impact on ammonia production, with ammonia concentration staying around 3700 ppm, which is more than three times higher than the plasma-only condition. Similarly, increases in Co loading had little to no effect on performance.

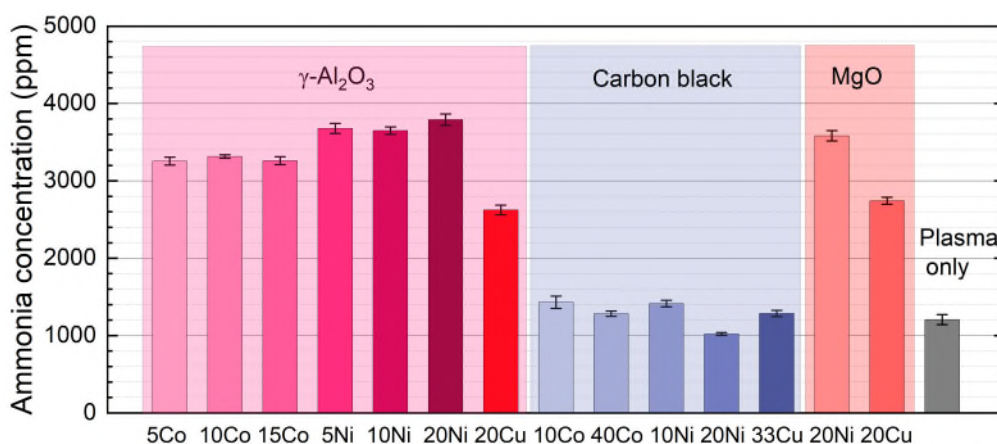


Figure 7. Ammonia concentration after the plasma reaction using transitional metals loaded $\gamma\text{-Al}_2\text{O}_3$, carbon black, and MgO, under fixed conditions: 8 W discharge power, 40 mL min^{-1} flow rate, and a 1:3 $\text{N}_2\text{:H}_2$ ratio.

These findings highlight the important role of catalyst support in plasma-catalytic ammonia production. The support material not only provides a structural framework for the active metal sites but also significantly influences reaction pathways through

factors such as metal dispersion, electron transfer, and interactions with the plasma. The choice of support material is therefore pivotal in optimizing catalyst performance and energy efficiency in plasma-assisted ammonia synthesis.

Effect of discharge power

Figure 8 illustrates the influence of discharge power on ammonia production using γ -Al₂O₃-based catalysts. An increase in discharge power led to higher ammonia yield rates under both plasma-only and plasma-catalyst conditions. Notably, loading Co and Ni onto γ -Al₂O₃ enhanced catalytic activity compared to the bare support, particularly at higher power levels. At a discharge power of 16 W, the ammonia yield rate with 10Ni/ γ -Al₂O₃ exceeded 5000 $\mu\text{mol g}^{-1} \text{h}^{-1}$, whereas γ -Al₂O₃ alone and plasma-only conditions achieved 4127 $\mu\text{mol g}^{-1} \text{h}^{-1}$ and 1865 $\mu\text{mol g}^{-1} \text{h}^{-1}$, respectively.

A comparison between γ -Al₂O₃-based catalysts and plasma-only conditions suggests that the catalytic activity is primarily governed by the support material rather than the loaded metal. This observation suggests a key distinction between plasma catalysis and conventional thermal catalysis. Unlike thermal processes, where the catalyst support is typically inert, plasma catalysis enables direct interactions between the plasma and the support, significantly influencing the overall catalytic effect.

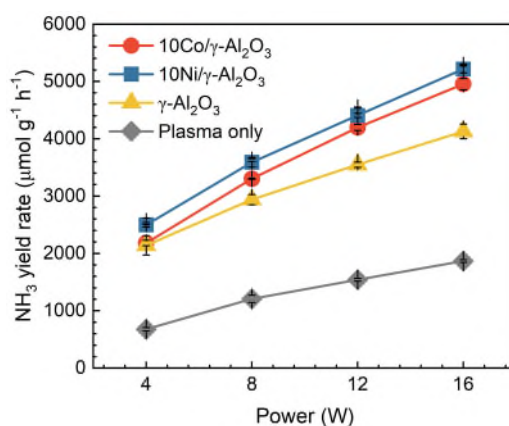


Figure 8. Ammonia production rate as a function of discharge power for 10 wt.% Co and Ni loaded γ -Al₂O₃, γ -Al₂O₃ support, and plasma only condition.

3.3.2 Performance of precious metals loaded support

Precious metals, such as Ru, have been extensively studied for plasma-catalytic ammonia synthesis and have shown promising results under specific conditions [15-

17]. In this study, Pt and Ru were selected as metal catalysts and supported on γ -Al₂O₃ and carbon black to investigate their role in plasma-enhanced ammonia production. However, as shown in Figure 4, the ammonia synthesis activity of Pt and Ru loaded γ -Al₂O₃ was similar to that of bare γ -Al₂O₃, suggesting that the addition of these metals did not significantly enhance catalytic performance.

This observation may indicate that ammonia production in this system is primarily driven by plasma-induced reactions rather than metal-mediated catalysis. Additionally, Pt and Ru may not effectively activate nitrogen on γ -Al₂O₃ and carbon black, or their interaction with the support may alter their catalytic properties, leading to suboptimal performance. Furthermore, the specific reaction conditions, such as plasma parameters, metal dispersion, and reaction temperature, could have influenced the observed results. Further investigations into alternative supports, optimized metal loadings, and tailored plasma conditions may be necessary to unlock the full potential of these metals for plasma-catalytic ammonia synthesis.

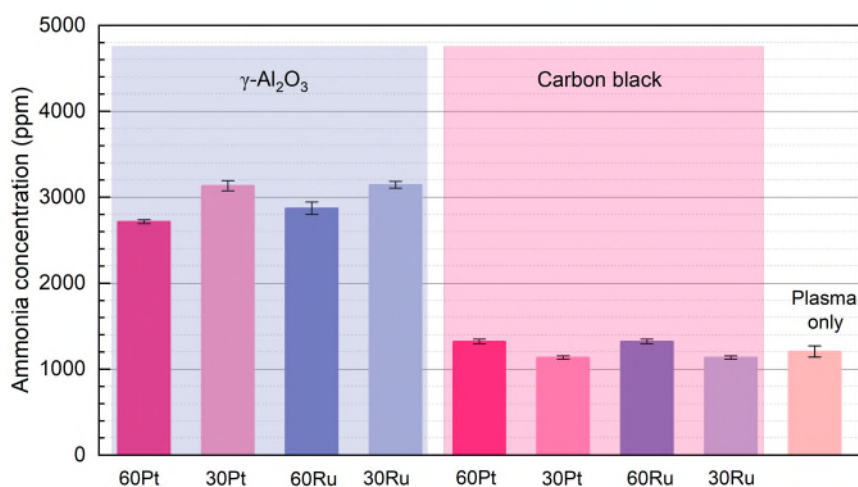


Figure 9. Ammonia concentration after the plasma reaction using precious metals loaded γ -Al₂O₃ and carbon black, under fixed conditions: 8 W discharge power, 40 mL min⁻¹ flow rate, and a 1:3 N₂:H₂ ratio.

3.4 Plasma-catalytic ammonia production from zeolite-based catalysts

3.4.1 Performance of Y-zeolite based catalysts

Transitional metals loaded catalysts

The choice of catalyst support plays a crucial role in optimizing reaction performance possibly by influencing metal dispersion, adsorption properties, and

plasma-catalyst interactions. Among various support materials, zeolites stand out due to their high surface area, tunable acidity, and favorable dielectric properties, which can enhance the generation of reactive nitrogen species and improve ammonia yield. This project first investigated the role of Y-zeolite as a support in plasma-catalytic ammonia synthesis. Different transitional metals and their combination were loaded on Y-zeolite to enhance its activity. Figure 10 shows the performance of these catalysts. Packing Y-zeolite into the discharge zone led to a notable improvement compared to the plasma-only condition. Loading transitional metals on Y-zeolite further promoted the performance, regardless of the type of transitional metals. Co, Ni, and Fe showed similar activity at the same loading. However, the combination of Fe and Ni led to a negative effect.

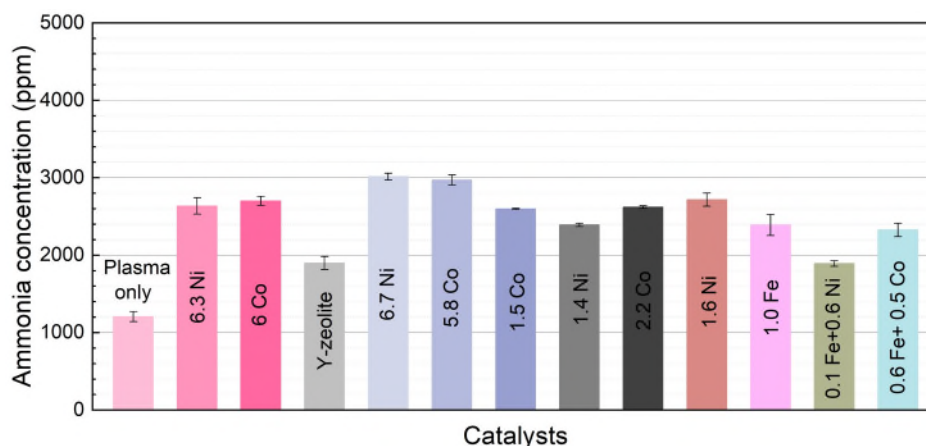


Figure 10. Ammonia concentration after the plasma reaction using transitional metals loaded Y-zeolite under fixed conditions: 8 W discharge power, 40 mL min⁻¹ flow rate, and a 1:3 N₂:H₂ ratio.

Effect of Ba and Ca promoters

The incorporation of Barium (Ba) and Calcium (Ca) as promoters in plasma-catalytic ammonia synthesis is intended to enhance nitrogen activation, modify catalyst properties, and stabilize active sites [17]. As strong electron donors, they facilitate N₂ dissociation and regulate hydrogenation, preventing catalyst deactivation. Additionally, their high dielectric constants improve plasma-catalyst interactions, while their oxides (BaO, CaO) contribute to thermal stability and reduce sintering. However, as shown in Figure 11, the catalysts containing Ba or Ca exhibited similar activity to those without a promoter, indicating that their anticipated benefits did not significantly enhance

ammonia production under the tested conditions.

Although Ba and Ca are known to improve catalytic performance in plasma-catalytic ammonia synthesis [17], their role in plasma-catalytic systems appears to be limited under the studied conditions. The results suggest that plasma effects may dominate the reaction mechanism, reducing the influence of traditional promoters. Further investigations are needed to optimize promoter loadings, catalyst-support interactions, and plasma parameters to determine whether Ba and Ca can contribute more effectively to enhancing ammonia production in plasma-driven processes.

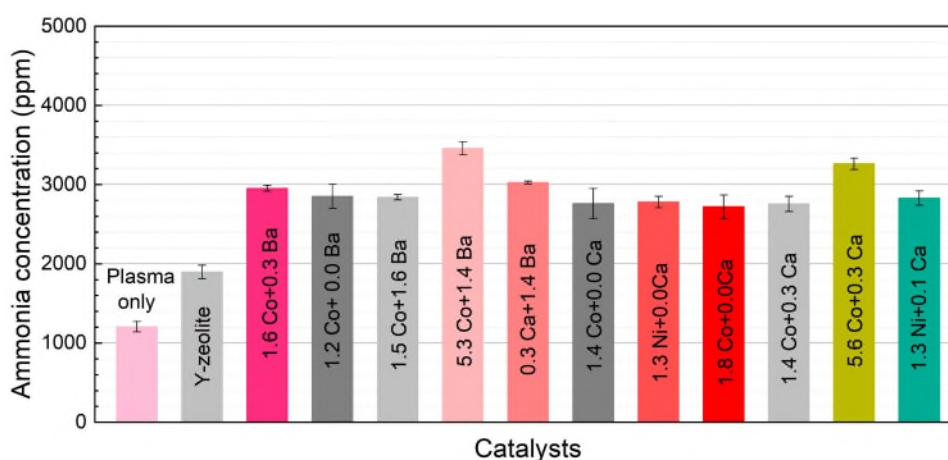


Figure 11. Ammonia concentration after the plasma reaction using Ba and Ca promoters incorporated transitional metals loaded Y-zeolite catalysts, under fixed conditions: 8 W discharge power, 40 mL min⁻¹ flow rate, and a 1:3 N₂:H₂ ratio.

Figure 12 presents the performance of Co-cluster and single-atom-modified Y-zeolite catalysts in plasma-catalytic ammonia production. However, neither modification strategy led to an enhancement in catalytic activity compared to the catalysts that had been tested previously. Notably, the 0.1% Co single-atom-modified Y-zeolite exhibited a detrimental effect, resulting in lower ammonia production than unmodified Y-zeolite. Bi-metallic catalysts incorporating Ba or Ca as promoters were investigated to further explore potential improvements. However, these bi-metallic systems did not yield any significant enhancement in performance, with ammonia concentrations consistently remaining around 3000 ppm.

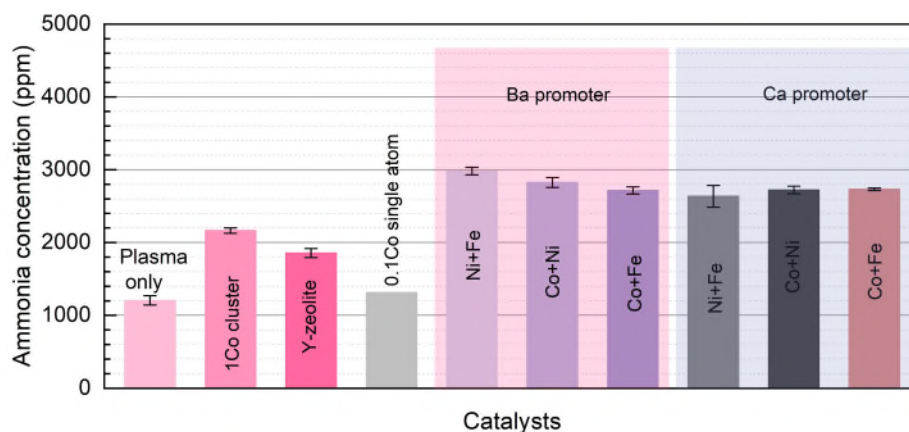


Figure 12. Ammonia concentration after the plasma reaction using Co cluster and Co single atom incorporated Y-zeolite, Ba and Ca promoters incorporated transitional metals loaded Y-zeolite catalysts, under fixed conditions: 8 W discharge power, 40 mL min⁻¹ flow rate, and a 1:3 N₂:H₂ ratio.

3.4.2 Performance of USY zeolite-based catalysts

The results indicate that the catalytic effect of metals supported on Y-zeolite is limited, likely due to weak metal-support interactions. To enhance ammonia production in the plasma-catalytic process, a range of zeolite materials were screened. Figure 8 presents the performance of the tested zeolites. Zeolites I, II, and III were derived from zeolite 4A via ion exchange, retaining the Linde-Type A (LTA) structure, which features a highly porous framework of interconnected cages and channels that facilitate efficient molecular sieving and adsorption. Zeolite IV, in contrast, possesses a Faujasite X-type structure with larger pore sizes than LTA zeolites. Among the tested materials, Zeolites I and III exhibited improved ammonia production compared to the plasma-only condition, while Zeolites II and IV had a negative impact. Specifically, at a discharge power of 8 W and a flow rate of 40 mL min⁻¹, Zeolite III achieved an ammonia concentration of approximately 3300 ppm, comparable to previous metal-loaded catalysts. In contrast, Zeolites II and IV resulted in ammonia concentrations below 1000 ppm.

Mordenite (MOR-type zeolite) was also evaluated as a potential support due to its high surface area, strong acidity, and excellent thermal stability. With a medium-to-high Si/Al ratio, mordenite offers a balance between Brønsted and Lewis acidity, which can enhance nitrogen activation while minimizing excessive hydrogen adsorption that

could poison the catalyst. However, Figure 13 shows that using mordenite as a catalyst lowered ammonia production, exhibiting similar performance to Zeolites II and IV.

Ultrastable Y (USY) zeolite, a modified form of Y-zeolite, was also investigated due to its enhanced thermal stability, optimized acidity, and improved catalytic performance. The dealumination process increases its Si/Al ratio, reducing excessive acidity while maintaining strong metal-support interactions. Three USY variants were tested: USY I (Si/Al = 10:1), USY II (Si/Al = 100), and USY III (Si/Al = 500). Interestingly, all USY zeolites outperformed Y-zeolite, with USY III demonstrating the highest activity, achieving an ammonia concentration exceeding 3700 ppm, which is three times higher than the plasma-only condition and twice that of γ -Al₂O₃. For USY materials, the higher Si/Al ratio, the higher activity in plasma-catalytic ammonia production process. A higher Si/Al ratio in USY zeolites could enhance plasma-catalytic ammonia synthesis by optimizing acidity, improving metal-support interactions, and strengthening plasma-catalyst interactions. These findings highlight the importance of zeolite structure and composition in plasma-catalytic ammonia synthesis, with USY zeolites showing significant potential for further optimization.

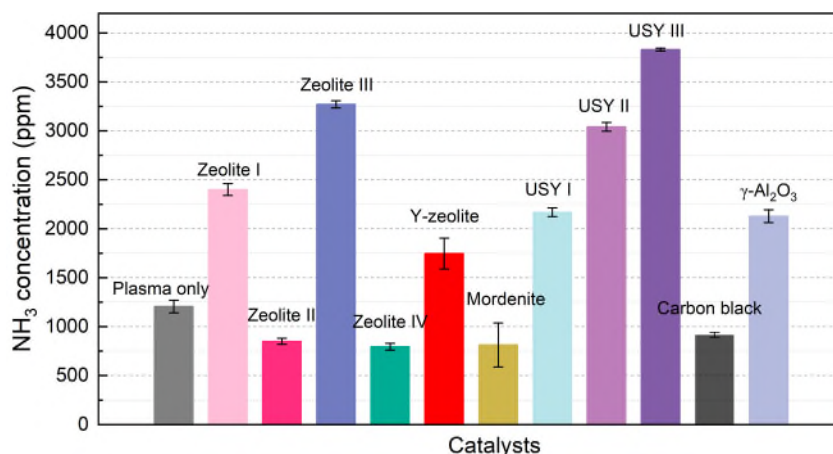


Figure 13. Ammonia concentration after the plasma reaction using various zeolite materials, under fixed conditions: 8 W discharge power, 40 mL min⁻¹ flow rate, and a 1:3 N₂:H₂ ratio.

Metal oxides loaded catalysts

Given the exceptional performance of USY III in plasma-catalytic ammonia synthesis, metal loading was explored to further enhance its activity. However, as seen in Figure 14, Fe₂O₃ exhibited negligible catalytic effects, while RuO₂ and RuO₂-Fe₂O₃

provided only limited improvements over the bare USY III support. In contrast, loading 3% NiO via the precipitation method significantly enhanced ammonia production to a concentration of 7277 ppm, highlighting the strong synergy between Ni and USY III under plasma conditions. Interestingly, increasing the NiO loading to 5% resulted in an activity similar to that of the unmodified USY III, suggesting an optimal NiO content for maximizing catalytic efficiency. Additionally, NiO loading via wetness impregnation also led to improved performance compared to the bare support, demonstrating that both the loading method and NiO concentration play crucial roles in optimizing the activity of the catalyst.

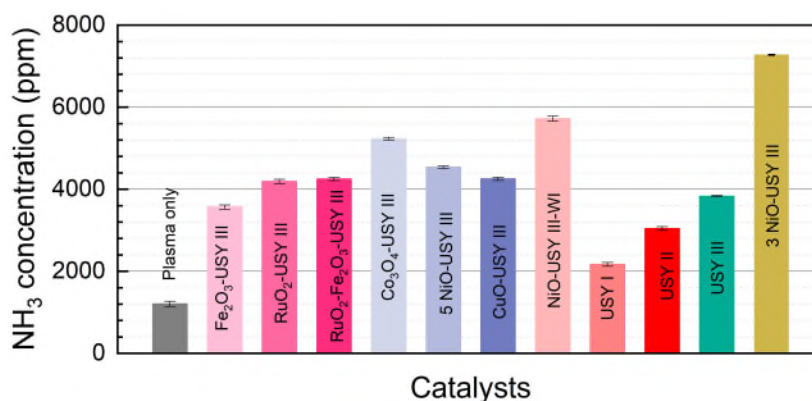


Figure 14. Ammonia concentration after the plasma reaction using various metals loaded USY III, under fixed conditions: 8 W discharge power, 40 mL min⁻¹ flow rate, and a 1:3 N₂:H₂ ratio.

Comparison of metal and metal oxides

Figure 15 compares transition metal oxides and their corresponding metal-loaded USY III catalysts in the plasma-catalytic ammonia synthesis process. The results indicate a variation in catalytic activity depending on the oxidation state of the transition metals. Specifically, for Fe, Co, and Ni-Co-based catalysts, the oxide forms exhibited notably higher performance than their metallic counterparts. This suggests that the presence of oxygen species might play a critical role in facilitating nitrogen activation and stabilizing reactive intermediates under plasma conditions. Metal oxides, particularly Fe₂O₃, Co₃O₄, and NiO, may enhance electron transfer dynamics and promote the formation of highly reactive nitrogen species for efficient ammonia synthesis. Additionally, metal oxides can provide stronger metal-support interactions, reducing the likelihood of catalyst deactivation through sintering or surface

reconstruction.

Conversely, in the case of copper-based catalysts, metallic Cu demonstrated slightly superior activity compared to CuO. This deviation from the trend observed with Fe, Co, and Ni-Co systems could be attributed to the unique electronic properties of Cu, which enable more efficient electron transfer between the plasma and catalytic surface, thereby enhancing nitrogen dissociation and subsequent hydrogenation to ammonia. Furthermore, the relatively low affinity of Cu for oxygen may limit the beneficial effects of oxide formation, making the metallic state more effective in plasma environments.

These findings indicate a relationship between oxidation state, plasma-catalyst interactions, and overall ammonia production efficiency. The superior performance of Fe, Co, and Ni-Co oxides highlights the potential of carefully tuning the oxidation state of transition metal catalysts to maximize plasma-catalytic activity. Moreover, the contrasting behavior of Cu-based catalysts suggests that different transition metals interact uniquely with plasma-generated species, necessitating further investigation to optimize catalyst design for enhanced ammonia synthesis.

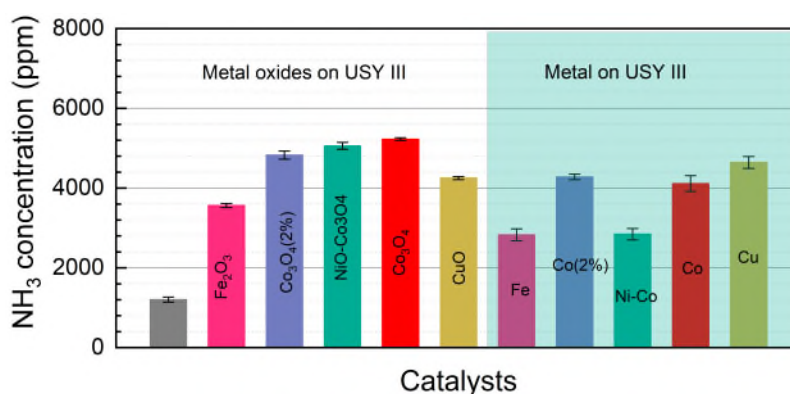


Figure 15. Ammonia concentration after the plasma reaction using metal oxides and metallic metal loaded USY III, under fixed conditions: 8 W discharge power, 40 mL min⁻¹ flow rate, and a 1:3 N₂:H₂ ratio.

Effect of discharge power:

Figure 16 illustrates the impact of discharge power on ammonia production for catalysts based on USY III. As the discharge power increased, there was a consistent enhancement in ammonia yield across all catalyst conditions. Notably, the increase in

discharge power had the most pronounced effect on the NiO-USY III catalyst, which achieved the highest ammonia yield rate of 18253 $\mu\text{mol g}^{-1} \text{h}^{-1}$. This suggests that the NiO-USY III catalyst is particularly responsive to higher discharge power, leading to a substantial improvement in ammonia production efficiency under the tested conditions.

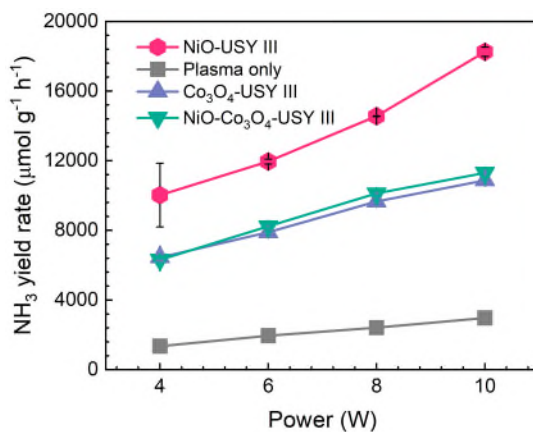


Figure 16. Ammonia production rate as a function of discharge power for NiO, Co₃O₄, and NiO-Co₃O₄ loaded USY III, and plasma-only condition.

3.4.3 Performance of zeolite III based catalysts

Effect of metal type and incorporation method

Among the various zeolite materials tested for plasma-catalytic ammonia production, zeolite III ranked second in terms of catalytic activity. Recognizing the potential for further enhancement, additional modifications were carried out to improve its performance. Specifically, different transition metals were loaded onto zeolite III using the wet impregnation method, a well-established technique that allows for uniform distribution of metals on the support. The results of these modifications revealed that cobalt (Co)-loaded zeolite III exhibited the highest catalytic activity, achieving an ammonia yield rate of 5373 $\mu\text{mol g}^{-1} \text{h}^{-1}$ (Figure 17). This was followed by nickel (Ni), iron (Fe), and copper (Cu), each of which also demonstrated improved ammonia production compared to unmodified zeolite III. While the catalytic activity varied between metals, all of the transition metals had a beneficial effect on the plasma-catalytic process, promoting higher ammonia yields than those observed with zeolite III alone.

To further enhance the catalytic performance, a more advanced technique, ion-

exchange, was employed to load Co onto zeolite III. This method allows for a more precise incorporation of metal ions into the zeolite structure, potentially improving the interaction between the metal and the zeolite framework, and leading to more effective catalysis. The Co-loaded zeolite III, prepared through ion-exchange, produced ammonia at an rate of $7352 \mu\text{mol g}^{-1} \text{h}^{-1}$, more than double the yield achieved using zeolite III without metal loading. This significant improvement indicates the critical role of metal loading techniques in optimizing the plasma-catalytic process and highlights the superior performance of Co when compared to other transition metals in this specific application.

These findings demonstrate that the choice of metal and the method of incorporation can have a huge impact on the activity of zeolite-based catalysts in plasma-catalytic ammonia production. The ion-exchange method, in particular, appears to be an effective strategy for enhancing the catalytic performance of zeolite III, offering the potential for more efficient and scalable ammonia production processes.

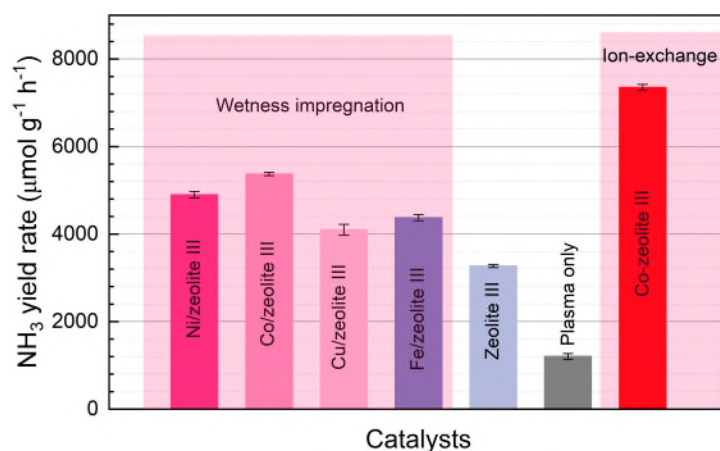


Figure 17. Ammonia concentration after the plasma reaction using metal-loaded zeolite III, under fixed conditions: 8 W discharge power, 40 mL min^{-1} flow rate, and a 1:3 $\text{N}_2:\text{H}_2$ ratio.

Stability test

In terms of stability, both zeolite III and Co-loaded zeolite III demonstrated long-term durability during a continuous 24-hour test, as illustrated in Figure 18. The results showed that these catalysts maintained a stable ammonia production rate over the entire duration of the experiment, with minimal degradation in performance. This suggests that both the zeolite III support material and the Co-modified version are well-suited

for extended use in plasma-catalytic ammonia production processes. The Co-loaded zeolite III, in particular, exhibited not only superior catalytic activity but also remarkable stability, indicating that the incorporation of cobalt did not negatively affect the long-term performance of the catalyst. These findings are crucial for evaluating the practical viability of these materials in real-world large-scale applications, where stability over extended periods is essential for efficient and cost-effective ammonia synthesis.

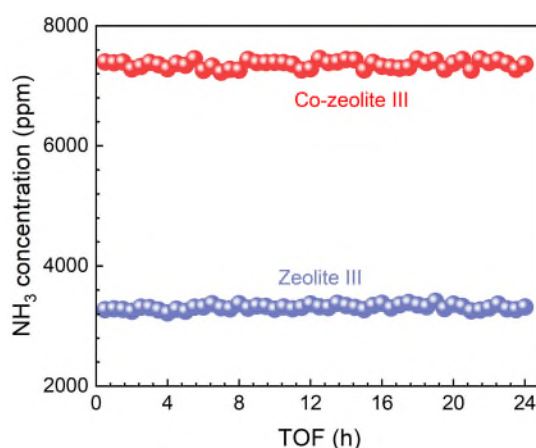


Figure 18. Stability test of Co-zeolite III and zeolite III in plasma-catalytic ammonia production process for 24 hours under fixed conditions: 8 W discharge power, 40 mL min⁻¹ flow rate, and a 1:3 N₂:H₂ ratio.

Effect of N₂:H₂ ratio

Previous results presented in Deliverable D4.1 demonstrated that the N₂:H₂ ratio plays a crucial role in influencing ammonia production in plasma-catalytic processes. To further optimize the plasma-catalytic reaction, a series of experiments were conducted at varying N₂:H₂ ratios. As shown in Figure 19, when zeolite III was used as the catalyst, the ammonia concentration peaked at a N₂:H₂ ratio of 1:1. This contrasts with the optimal N₂:H₂ ratio in plasma-only conditions, which was found to be 1:2. The introduction of Co-loaded zeolite III as the catalyst resulted in a shift in the optimal N₂:H₂ ratio, with the highest ammonia concentration observed at a ratio of 2:1. These findings highlight the significant influence of the N₂:H₂ ratio on ammonia synthesis, indicating that the presence of Co in the catalyst modifies the reaction pathway, thereby enhancing the overall efficiency of ammonia production under specific gas mixture

conditions. A high $N_2:H_2$ ratio for ammonia production is advantageous in industrial applications because it can help reduce the amount of hydrogen needed, which is often the more expensive and energy-intensive reactant to produce. In many industrial processes, hydrogen is sourced from natural gas or other fossil fuels, which incurs high costs and carbon emissions. By increasing the nitrogen content relative to hydrogen, the process can make better use of abundant and relatively inexpensive nitrogen, reducing the reliance on hydrogen. This adjustment also helps in optimizing the reaction conditions, making the ammonia synthesis process more cost-effective and potentially more sustainable. Additionally, a higher $N_2:H_2$ ratio can improve the overall efficiency of plasma-catalytic systems, leading to enhanced ammonia production with lower energy consumption, which is highly beneficial for large-scale industrial operations looking to improve both productivity and energy efficiency.

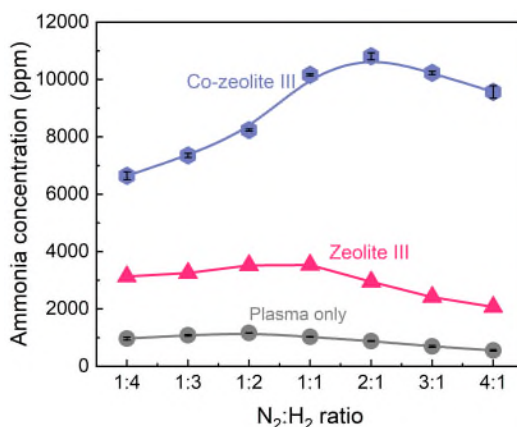


Figure 19. Effect of $N_2:H_2$ ratio on ammonia production using Co-zeolite III and zeolite III as catalysts.

In terms of energy efficiency, the highest energy yield for ammonia production was achieved using Co-loaded zeolite III as the catalyst (Figure 20). Under optimal conditions, including a discharge power of 8W, a flow rate of 40 mL min^{-1} , and a $N_2:H_2$ ratio of 2:1, the Co-zeolite catalyst produced an impressive energy yield of 2.25 g kWh^{-1} . This result is particularly noteworthy because it demonstrates a highly efficient conversion of electrical energy into ammonia, which is essential for scaling up the process in industrial applications where energy costs are a significant factor.

When compared to the same conditions without the Co-zeolite catalyst, the energy

yield was substantially lower (0.18 g kWh^{-1}). This contrast highlights the crucial role that the catalyst plays in enhancing the overall energy efficiency of the ammonia production process. The Co-zeolite catalyst significantly improved the conversion efficiency by facilitating the plasma-catalytic reaction, thereby enabling a higher ammonia output for the same input of electrical power.

This result also highlights the importance of optimizing catalyst properties and reaction conditions in plasma-assisted ammonia synthesis. The use of Co-loaded zeolite not only boosts ammonia production rates but also enhances the energy efficiency of the entire system, making it a more viable and sustainable option for large-scale ammonia production. By improving the energy yield, it becomes possible to reduce the operational costs and environmental impact of ammonia synthesis, aligning with the growing demand for more energy-efficient and eco-friendly industrial processes.

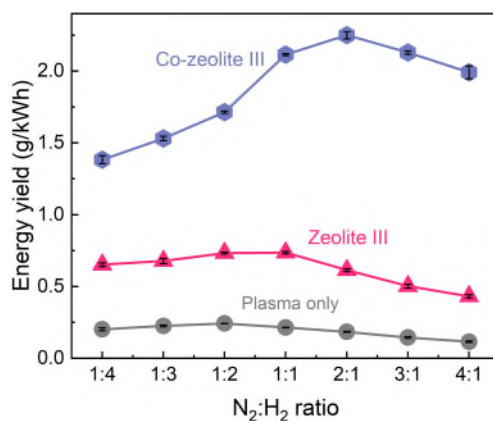


Figure 20. Effect of N₂:H₂ ratio on energy yield of ammonia production using Co-zeolite III and zeolite III as catalysts.

3.5 Understanding plasma-catalytic ammonia production mechanism based on zeolite materials

3.5.1 Performance of zeolite I, II, III, and IV

The significant differences in the catalytic activity of zeolites I, II, III, and IV provide valuable insights into the underlying mechanism. In this study, we examined the effect of discharge power on plasma-catalytic ammonia production while keeping all other parameters constant. As shown in Figure 21(a), increasing the power led to higher ammonia concentrations and NH₃ yield rates across all tested zeolites. This enhancement can be attributed to the generation of more active species at higher power

levels, which are essential for NH_3 formation. Specifically, increasing plasma discharge power results in a greater number of energetic electrons, which interact with atoms and molecules to produce the reactive species necessary for ammonia synthesis.

The positive effect of increased power was particularly pronounced for zeolites II and IV, where ammonia concentrations rose more than tenfold as the power increased from 4 W to 16 W. For instance, with zeolite II, the ammonia concentration increased from 144.8 ppm to 2517.7 ppm under these conditions. Notably, while zeolites II and IV initially exhibited an inhibitory effect on ammonia production, this shifted to a catalytic enhancement when the power exceeded 12 W. Despite these variations, the highest ammonia production rate ($536.9 \mu\text{mol g}^{-1} \text{h}^{-1}$) was achieved with zeolite III at the maximum power of 16 W.

Figure 21(b) illustrates the relationship between discharge power and NH_3 production energy yield. For zeolites I and III, energy yield decreased with increasing power, mirroring the trend observed under plasma-only conditions. This negative effect of high power on plasma-catalytic reactions is well-documented in the literature [7, 8, 18-20]. The decline in energy yield can be attributed to the excessive generation of electrons at higher power levels, many of which fail to effectively collide with target molecules (N_2 and H_2), resulting in energy loss and reduced overall efficiency.

However, this explanation does not fully account for the contrasting behavior observed with zeolites II and IV, where energy yield increased at higher power levels. As shown in Figure 21(d), the energy yield for NH_3 production with zeolite II rose from 0.06 g kWh^{-1} to 0.26 g kWh^{-1} as power increased from 4 W to 16 W. Despite this improvement, the energy efficiency achieved with zeolites II and IV remained lower than that of zeolites I and III across all tested power levels.

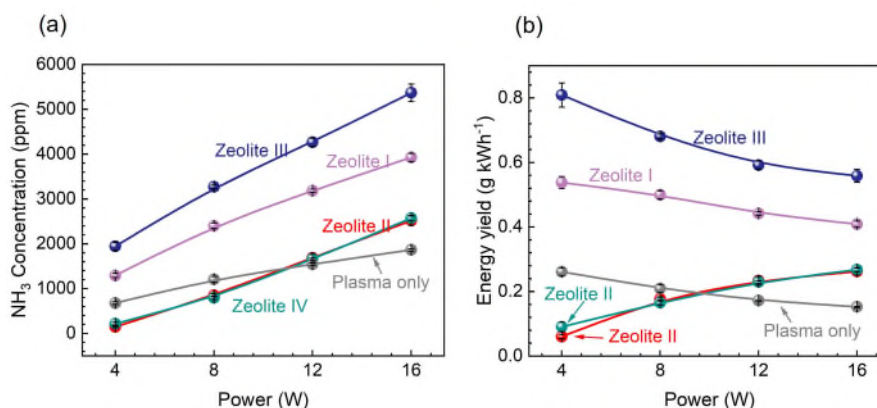


Figure 21. Effect of discharge power on (a) ammonia concentration and (b) energy yield of ammonia production using zeolite I, II, III, and IV as catalysts.

3.5.2 Characterizations of zeolite I, II, III, and IV

The X-ray diffraction (XRD) profiles of zeolites I, II, III, and IV (Figure 22) confirm their crystalline purity and phase integrity, as no additional peaks indicative of impurities or secondary phases are observed. The XRD patterns of zeolites I, II, and III align with the characteristic cubic structure of Linde-Type A (LTA) zeolite, which belongs to the space group $Fm\bar{3}c$. This highly porous framework consists of interconnected cages and channels, facilitating efficient molecular sieving and adsorption [21].

In contrast, zeolite IV exhibits an XRD pattern characteristic of Faujasite X-type zeolite, which crystallizes in a cubic structure with space group $Fd\bar{3}m$. Faujasite zeolites are distinguished by their larger pore sizes compared to LTA zeolites, which can significantly influence their adsorption behavior and interactions with gas molecules [22].

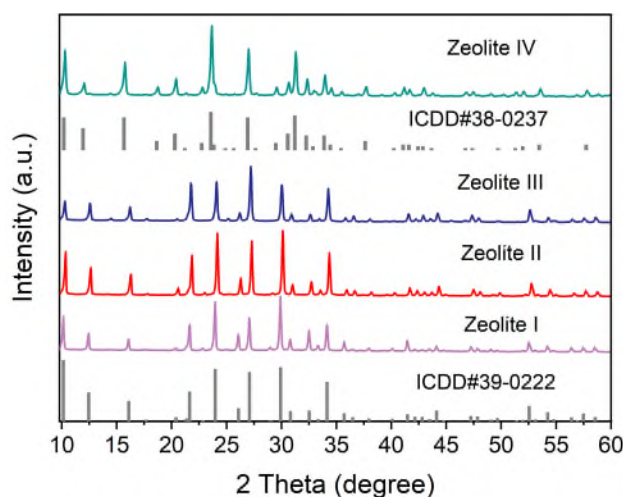


Figure 22. XRD results of zeolite I, II, III, and IV.

Figure 23 presents SEM images of the zeolite materials, further confirming their well-defined cubic morphology. The uniform cubic crystals observed in zeolites I, II, III, and IV highlight their structural consistency, which is essential for ensuring reproducibility and reliability in catalytic applications. Notably, while all zeolites exhibit distinct and regular crystalline forms, zeolite IV tends to have smaller crystals compared to the LTA-type zeolites.

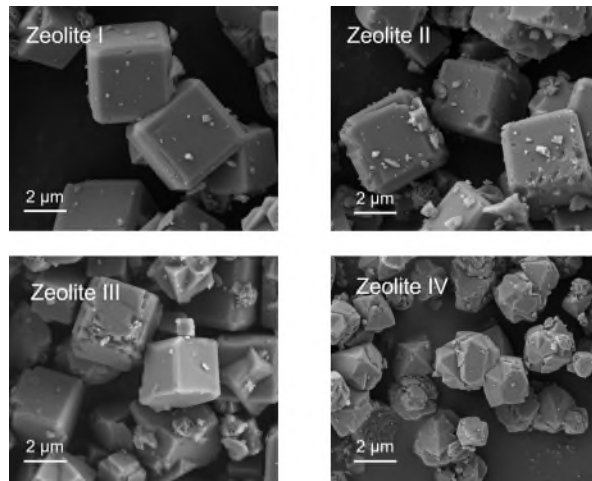


Figure 23. SEM images of zeolite I, II, III, and IV

The EDX results in Table 2 summarize the elemental composition of the zeolite materials. The Al/Si ratio remains approximately 1 across all samples. In addition to aluminum and silicon, sodium is present in all zeolites, with molar percentages ranging from 11.7% in zeolite III to 32.9% in zeolite II.

Zeolites I and III are typically synthesized through ion exchange, where Na^+ is partially replaced by K^+ and Ca^{2+} within the LTA structure (Si/Al ratio = 1) [23], a finding corroborated by our EDX analysis. Additionally, the EDX results confirm that the Faujasite X-type structure of zeolite IV (Si/Al ratio = 1.2) predominantly contains Na^+ [24].

Table 2. EDX elemental analysis of different zeolite materials

at. % (C, O excluded)	Al	Si	Na	K	Ca
Zeolite I	3	32.0	19.4	15.0	
Zeolite II	3	32.9	32.9		
Zeolite III	3	36.0	11.7		14.7
Zeolite IV	3	38.1	30.1		

Figure 24(a) presents the NH_3 -TPD results for the zeolite materials, revealing distinct

desorption profiles. In Figure 24(b), the relative ammonia adsorption capacities of the zeolites are compared based on desorption intensity. Zeolite III exhibited the highest ammonia adsorption capacity, followed by zeolite IV, zeolite II, and zeolite I.

However, the catalytic activity, ranked as zeolite III > zeolite I > zeolite II \approx zeolite IV, suggests that higher ammonia adsorption capacity does not necessarily translate to greater catalytic performance. For instance, although zeolite IV adsorbed nearly twice as much ammonia as zeolite I, the latter demonstrated higher activity. To investigate this discrepancy, we further analyzed the acid properties of the zeolites through deconvolution of the NH₃-TPD data, which will be discussed later.

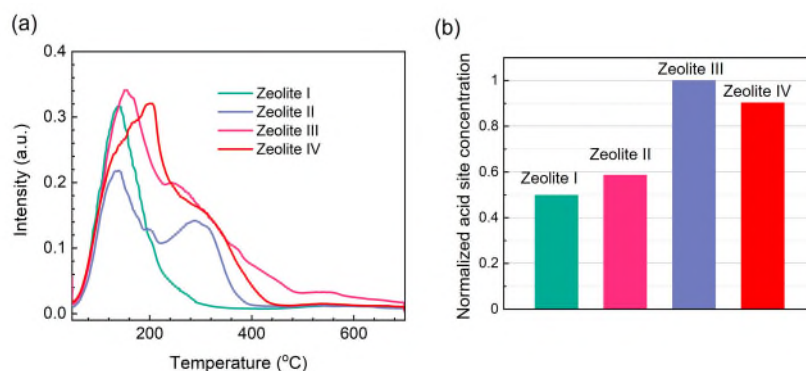


Figure 24. (a) NH₃-TPD results and (b) normalized acid site concentration of zeolite I, II, III, and

IV

3.5.3 Characterization of plasma-catalysis discharge

Discharge signals

As previously discussed, the varying effects of zeolites on plasma-catalytic ammonia production may be attributed to differences in plasma discharge characteristics. To explore this further, we analyzed the electrical signals of the discharge. As shown in Figure 25(a), the peak-to-peak voltage across the electrodes remained around 16 kV, regardless of the packing material.

Current spikes, indicative of micro-discharges [25, 26], were observed, with the corresponding current profiles presented in Figure 25(b). While micro-discharges occurred in all cases, they were significantly stronger under plasma-only conditions. In the dielectric barrier discharge (DBD) system without packing material (plasma only), micro-discharges spanned the entire discharge gap, extending from the inner electrode to the dielectric surface. However, when the gap was packed with catalyst support, the micro-discharges could no longer propagate freely. Instead, the available space for

filamentary micro-discharge formation became restricted, resulting in fewer filamentary micro-discharges and an increased occurrence of surface discharges [25, 26]. This explains the weaker micro-discharges observed in DBD reactors packed with zeolite materials compared to the plasma-only condition.

A higher number of micro-discharges could potentially enhance plasma-assisted reactions [27]. However, discharge characteristics do not fully explain the superior performance of zeolite I relative to zeolites II and IV, nor do they account for the observed trends in ammonia (NH_3) yield rates and energy efficiency.

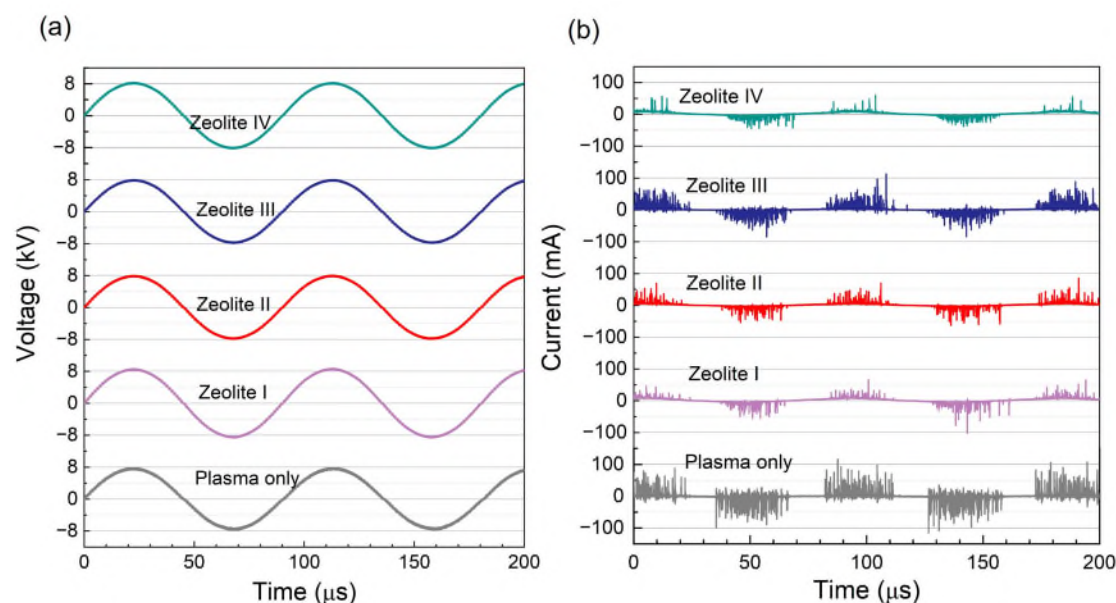


Figure 25. Comparison of (a) discharge voltage and (b) discharge current when packing zeolite I, II, III, and IV in the discharge area.

OES diagnosis of plasma

Figure 26 presents the OES spectra obtained when different zeolite materials were introduced into the plasma-catalytic system. Across all conditions, the spectra primarily feature emissions from the second positive system of nitrogen (N_2 , SPS), the first negative system of nitrogen ions (N_2^+ , FNS), the first positive system of nitrogen (N_2 , FPS), the hydrogen atom (H_α), and the nitrogen atom ($3p^2p^0 - 3s^2p$). These signals indicate electronic excitation and ionization of N_2 , as well as the dissociation of N_2 and H_2 in the N_2 - H_2 plasma.

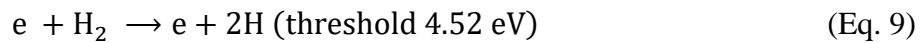
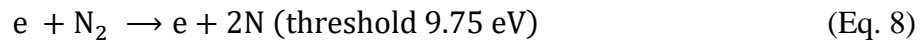
The overall spectral intensity follows the order: plasma only \approx zeolite I $>$ zeolite III $>$ zeolite IV $>$ zeolite II, which does not directly correlate with the observed performance trends. The stronger OES signals observed with zeolites I and III suggest that these

materials interact more significantly with the plasma, facilitating enhanced gas-phase excitation and energy transfer.

To compare the relative intensities of hydrogen and nitrogen emissions, the nitrogen atom spectra were normalized, as shown in Figure 26(b). Zeolite I exhibited the highest H/N intensity ratio, followed by zeolite II, zeolite IV, zeolite III, and the plasma-only condition. A higher H/N ratio suggests a greater extent of hydrogen dissociation compared to nitrogen dissociation, implying that the catalyst is more effective at breaking H₂ bonds than N₂ bonds. Alternatively, as proposed by Wang et al. [28], a higher fraction of H atoms could result from the enhanced adsorption of nitrogen atoms on the zeolite surface.

Energetic electrons within the plasma dissociate N₂ and H₂ molecules into atoms (N and H) through electron-molecule collisions under strong electric fields (see Eq. (8) and (9)). While no clear relationship exists between catalytic performance and the N/H ratio, zeolite III, which exhibited a high N/H ratio, demonstrated the best performance among the tested zeolites. This is likely due to its enhanced ability to promote N₂ dissociation, a key step in plasma-enhanced catalytic ammonia synthesis [29].

Figure 26(c) compares the relative intensity of NH to N₂(0,0). Among all tested zeolites, only zeolite I exhibited an increased NH intensity relative to the plasma-only condition, whereas all other materials showed nearly identical NH intensities.



The intensity ratio between the N₂⁺(0,0) (391.4 nm) and N₂(2,5) (394.3 nm) emissions in optical emission spectroscopy (OES) serves as a key diagnostic tool for analyzing plasma characteristics. Both emissions originate from the interaction of metastable nitrogen molecules [30]. An increase in the N₂⁺ (391.4 nm) to N₂ (394.3 nm) ratio indicates enhanced ionization, potentially driven by stronger electric fields near the surface of zeolite materials [31].

Among the tested zeolites, Zeolite IV exhibits the highest N₂⁺(0,0)/N₂(2,5) ratio, suggesting that its surface facilitates the generation of high-energy electrons, thereby promoting ionization over neutral excitation. Conversely, despite showing the highest catalytic activity, Zeolite III presents the lowest N₂⁺(0,0)/N₂(2,5) ratio. This observation implies that neutral excitation might play a more significant role in plasma-catalytic ammonia production.

Interestingly, performance trends reveal that neither a higher spectral intensity nor a specific $N_2^+(0,0)/N_2(2,5)$ ratio directly correlates with ammonia production efficiency. This discrepancy suggests that factors beyond gas-phase excitation, such as the surface properties of zeolite, their ability to adsorb and activate reactants, and their role in stabilizing reactive intermediates, may play a more decisive role in determining catalytic activity.

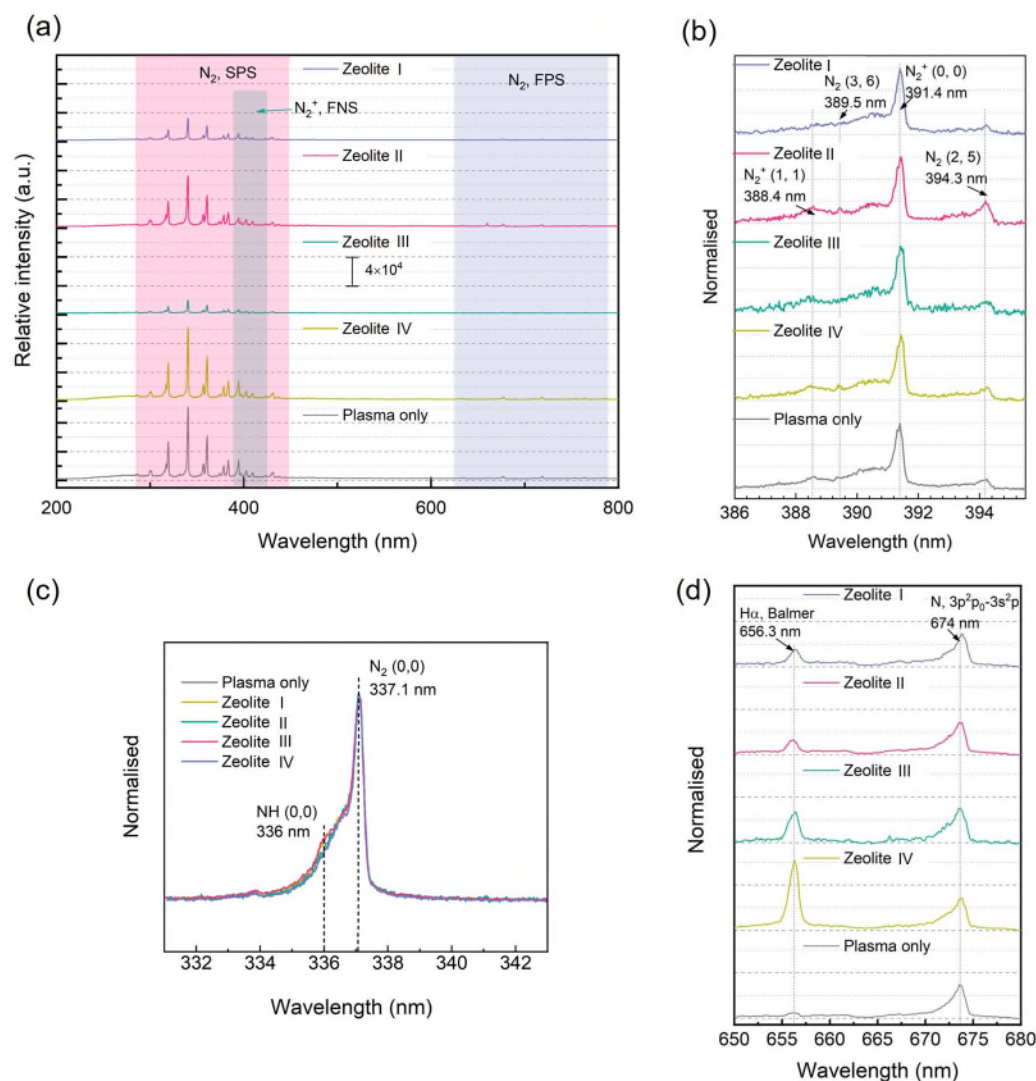


Figure 26. Comparison of (a) broad scope OES spectra (200 - 800 nm), (b) the spectra of the H atom and the N atom by normalizing the N atom spectra, (c) $NH(0,0)$ spectra by normalizing $N_2(0,0)$, and (d) the spectra of the $N_2^+(0,0)$ (391.4 nm) and $N_2(2,5)$ (394.3 nm) by normalizing $N_2^+(0,0)$, using zeolite I, II, III, and IV as the catalyst.

3.5.4 Proposed mechanism based on NH_3 -TPD results

Figure 27 presents the deconvoluted NH₃-TPD results, where the fitted peaks are categorized into three groups based on desorption and plasma temperatures: weak acid sites (peaking below 210 °C), medium acid sites (peaking between 210 °C and 275 °C), and strong acid sites (peaking above 275 °C). This classification helps differentiate the various NH₃ desorption sites on the catalysts. Zeolite I primarily consists of weak and medium acid sites, with the intensity of the weak acid sites significantly exceeding that of the medium acid sites.

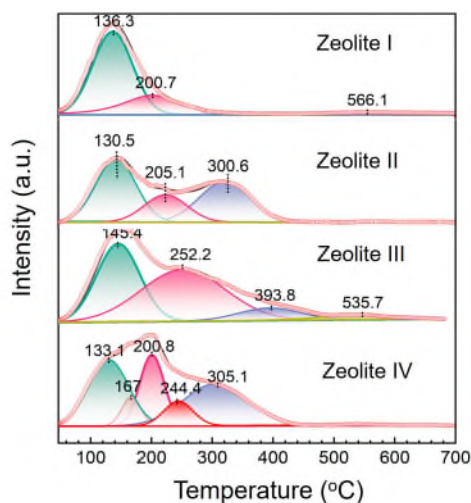


Figure 27. Deconvoluted NH₃-TPD results of zeolite I, II, III, and IV.

Given the operating temperature of the DBD reactor, it is hypothesized that ammonia formed during the catalytic reaction cannot be adsorbed onto weak acid sites. Consequently, materials composed solely of weak acid sites do not contribute to ammonia production, as they lack the ability to retain ammonia generated in the plasma-catalytic reaction.

In contrast, materials containing medium and strong acid sites can adsorb ammonia from the gas phase into the zeolite pores under plasma conditions. This adsorption creates a "shielding effect," protecting the formed ammonia and shifting the equilibrium toward increased ammonia production. However, if a material contains only strong acid sites, the adsorbed ammonia is unlikely to desorb, particularly at low power levels. Moreover, high-energy electrons may interact with the ammonia adsorbed on the zeolite surface, negatively impacting ammonia production.

On the other hand, ammonia adsorbed on medium acid sites desorbs more readily. This suggests that medium acid sites enhance ammonia production by capturing the formed ammonia near its generation sites while preventing surface decomposition.

The results supported this assumption. For zeolite I, the presence of a few medium acid sites and the absence of strong acid sites enhanced ammonia production compared to plasma treatment alone. In contrast, when the DBD reactor was packed with zeolite II or zeolite IV, ammonia production decreased at discharge powers below 12 W. This reduction was attributed to the high concentration of strong acid sites in these zeolites and the relatively low number of medium acid sites. However, increasing the discharge power mitigated this negative effect, as higher temperatures and more energetic electrons facilitated ammonia desorption. Among the tested zeolites, zeolite III, which has a high density of medium acid sites and significantly fewer strong acid sites, was expected to perform best, a prediction confirmed by the results.

4. Collusion

In this deliverable, we first presented a detailed kinetic model for plasma-assisted ammonia synthesis. This model encompasses a variety of electron impact reactions, reactions involving excited species, ionic reactions, and chemical reactions between neutral species. The model is validated by comparing the model predictions and experimentally measured steady-state data of ammonia concentration as a function of input power. The model prediction shows a good agreement with the experimental data, confirming the validity of the designed plasma chemical kinetics model. The path flux analysis was conducted to elucidate the underlying mechanism of ammonia synthesis at 40 mL min⁻¹ and 8 W input power. The simulation results show that ammonia is primarily formed through the recombination reactions $\text{NH}_2 + \text{H} + \text{M} \rightarrow \text{NH}_3 + \text{M}$ and $\text{NH} + \text{H}_2 + \text{M} \rightarrow \text{NH}_3 + \text{M}$. Meanwhile, the formation of NH and NH₂ radicals is attributed to the successive hydrogenation of N and N(²D). These findings provide new insights into improving the ammonia formation for the plasma-assisted ammonia synthesis process.

The experimental studies highlight the significant impact of catalyst support materials and metal loadings on plasma-catalytic ammonia production. The performance of non-zeolite-based catalysts, such as $\gamma\text{-Al}_2\text{O}_3$, carbon black, and MgO, demonstrates the critical role of support materials in optimizing catalytic activity, electron transfer, and metal dispersion. Among these, $\gamma\text{-Al}_2\text{O}_3$ proved to be the most effective support,

promoting substantial improvements in ammonia yield through efficient metal dispersion and strong interactions with the plasma. Notably, the catalytic performance was highly influenced by the discharge power, with γ -Al₂O₃-based catalysts showing remarkable enhancements when combined with metals like Ni and Co, underscoring the importance of careful selection and optimization of both the support and metal catalyst.

The incorporation of transition metals such as Ru and Pt, supported on γ -Al₂O₃ and carbon black, did not significantly enhance ammonia production, suggesting that plasma-driven processes may primarily rely on plasma-induced reactions rather than metal-catalyzed steps. This highlights a key distinction between plasma-catalytic and conventional thermal catalytic processes, where the role of support materials is more pronounced in plasma systems due to direct plasma-support interactions.

Further investigation into zeolite-based catalysts revealed that Y-zeolite, along with various metal and promoter modifications, showed promising potential in enhancing ammonia production. Particularly, USY zeolite exhibited significant improvements in ammonia yield, with a notable synergy observed when combined with NiO. The results from zeolite III, both in its unmodified form and as modified with Co through ion-exchange, showed remarkable catalytic activity and stability, establishing its potential for large-scale applications. Additionally, the optimization of the N₂:H₂ ratio demonstrated that Co-loaded zeolite III could shift the optimal conditions, enhancing ammonia production efficiency and reducing hydrogen consumption, which is crucial for economic and environmental sustainability in industrial ammonia synthesis.

The study also demonstrated the importance of energy efficiency in plasma-catalytic processes. The Co-loaded zeolite III catalyst achieved the highest energy yield of 2.25 g kWh⁻¹, emphasizing the potential of plasma-assisted ammonia synthesis for industrial-scale applications where energy costs are a major consideration.

Regarding the underlying mechanism, we have demonstrated that the characteristics of acid sites play a crucial role in the catalytic performance of zeolite materials in plasma-catalytic ammonia synthesis. Our results show that zeolite III,

which is rich in medium acid sites, enhances NH₃ production by facilitating efficient adsorption and desorption processes. In contrast, zeolites with a high concentration of strong acid sites impede ammonia desorption, reducing their catalytic efficiency, especially at lower discharge powers.

In summary, the project highlights the importance of selecting the right catalyst support, metal loading, and plasma conditions to optimize ammonia production. It also highlights the promising potential of Co and Ni-loaded zeolites, particularly USY zeolite and tailored LTA zeolite, for enhancing energy efficiency and ammonia yield. The insights into the mechanisms governing plasma-catalytic ammonia synthesis emphasize the importance of rational catalyst design that prioritizes the balance of acid site types. These findings provide valuable insights into advancing plasma-catalytic ammonia synthesis, paving the way for more sustainable and efficient industrial processes.

Reference

- [1] C. Smith, A.K. Hill, L. Torrente-Murciano, Current and future role of Haber–Bosch ammonia in a carbon-free energy landscape, *Energy & Environmental Science* 13(2) (2020) 331-344.
- [2] M.R. Moghadam, A. Bazmandegan-Shamili, H. Bagheri, The current methods of ammonia synthesis by Haber-Bosch process, *Progresses in Ammonia: Science, Technology and Membranes*, Elsevier2024, pp. 1-32.
- [3] M. Wang, M.A. Khan, I. Mohsin, J. Wicks, A.H. Ip, K.Z. Sumon, C.-T. Dinh, E.H. Sargent, I.D. Gates, M.G. Kibria, Can sustainable ammonia synthesis pathways compete with fossil-fuel based Haber–Bosch processes?, *Energy & Environmental Science* 14(5) (2021) 2535-2548.
- [4] P. Peng, P. Chen, C. Schiappacasse, N. Zhou, E. Anderson, D. Chen, J. Liu, Y. Cheng, R. Hatzenbeller, M. Addy, A review on the non-thermal plasma-assisted ammonia synthesis technologies, *Journal of cleaner production* 177 (2018) 597-609.
- [5] J. Zhang, X. Li, J. Zheng, M. Du, X. Wu, J. Song, C. Cheng, T. Li, W. Yang, Non-thermal plasma-assisted ammonia production: A review, *Energy Conversion and Management* 293 (2023) 117482.
- [6] S. Samipour, M.R. Rahimpour, Nonthermal plasma-assisted ammonia synthesis technologies, *Progresses in Ammonia: Science, Technology and Membranes*, Elsevier2024, pp. 33-62.
- [7] G. Zhou, H. Zhao, X. Wang, Z. Wang, Y. Zhang, X. Zhao, Q. Chen, T. Chen, Z. Huang, H. Lin, Plasma-catalytic ammonia synthesis on Ni catalysts supported on Al₂O₃, Si-MCM-41 and SiO₂, *International Journal of Hydrogen Energy* 60 (2024) 802-813.

- [8] Y. Wang, M. Craven, X. Yu, J. Ding, P. Bryant, J. Huang, X. Tu, Plasma-Enhanced Catalytic Synthesis of Ammonia over a Ni/Al₂O₃ Catalyst at Near-Room Temperature: Insights into the Importance of the Catalyst Surface on the Reaction Mechanism, *ACS Catal* 9(12) (2019) 10780-10793. <https://doi.org/10.1021/acscatal.9b02538>.
- [9] X. Zhu, X. Hu, X. Wu, Y. Cai, H. Zhang, X. Tu, Ammonia synthesis over γ -Al₂O₃ pellets in a packed-bed dielectric barrier discharge reactor, *Journal of Physics D: Applied Physics* 53(16) (2020) 164002.
- [10] B.S. Patil, A.S. Van Kaathoven, F.J. Peeters, N. Cherkasov, J. Lang, Q. Wang, V. Hessel, Deciphering the synergy between plasma and catalyst support for ammonia synthesis in a packed dielectric barrier discharge reactor, *Journal of Physics D: Applied Physics* 53(14) (2020) 144003.
- [11] J.R. Shah, F. Gorky, J. Lucero, M.A. Carreon, M.L. Carreon, Ammonia synthesis via atmospheric plasma catalysis: zeolite 5A, a case of study, *Industrial & Engineering Chemistry Research* 59(11) (2020) 5167-5176.
- [12] K.H. Rouwenhorst, S. Mani, L. Lefferts, Improving the energy yield of plasma-based ammonia synthesis with in situ adsorption, *ACS sustainable chemistry & engineering* 10(6) (2022) 1994-2000.
- [13] F. Gorky, M.A. Carreon, M.L. Carreon, Experimental strategies to increase ammonia yield in plasma catalysis over LTA and BEA zeolites, *IOP SciNotes* 1(2) (2020) 024801.
- [14] F. Gorky, A. Nambo, M.A. Carreon, M.L. Carreon, Plasma catalytic conversion of nitrogen and hydrogen to ammonia over silico alumino phosphate (SAPO) zeolites, *Plasma Chemistry and Plasma Processing* 44(3) (2024) 1357-1368.
- [15] J. Liu, X. Zhu, S. Jiang, H. Zhang, Y. Hong, G. Chen, X. Tu, Plasma-catalytic synthesis of ammonia over Ru/BaTiO₃-based bimetallic catalysts: Synergistic effect from dual-metal active sites, *Fuel Processing Technology* 250 (2023) 107851.
- [16] X. Zhu, J. Liu, X. Hu, Z. Zhou, X. Li, W. Wang, R. Wu, X. Tu, Plasma-catalytic synthesis of ammonia over Ru-based catalysts: Insights into the support effect, *Journal of the Energy Institute* 102 (2022) 240-246.
- [17] H.H. Kim, Y. Teramoto, A. Ogata, H. Takagi, T. Nanba, Atmospheric-pressure nonthermal plasma synthesis of ammonia over ruthenium catalysts, *Plasma Processes and Polymers* 14(6) (2017) 1600157.
- [18] D. Mei, X. Zhu, C. Wu, B. Ashford, P.T. Williams, X. Tu, Plasma-photocatalytic conversion of CO₂ at low temperatures: understanding the synergistic effect of plasma-catalysis, *Applied Catalysis B: Environmental* 182 (2016) 525-532.
- [19] D. Mei, X. Zhu, Y.-L. He, J.D. Yan, X. Tu, Plasma-assisted conversion of CO₂ in a dielectric barrier discharge reactor: understanding the effect of packing materials, *Plasma Sources Science and Technology* 24(1) (2014) 015011.
- [20] X. Zeng, S. Zhang, Y. Liu, X. Hu, K.K. Ostrikov, T. Shao, Energy-efficient pathways for pulsed-plasma-activated sustainable ammonia synthesis, *ACS Sustainable Chemistry & Engineering* 11(3) (2023) 1110-1120.
- [21] K. Aoki, K. Kusakabe, S. Morooka, Separation of gases with an A-type zeolite membrane, *Industrial & engineering chemistry research* 39(7) (2000) 2245-2251.
- [22] H. Lechert, H. Kacirek, Investigations on the crystallization of X-type zeolites,

Zeolites 11(7) (1991) 720-728.

[23] F. Hasan, R. Singh, G. Li, D. Zhao, P.A. Webley, Direct synthesis of hierarchical LTA zeolite via a low crystallization and growth rate technique in presence of cetyltrimethylammonium bromide, *Journal of colloid and interface science* 382(1) (2012) 1-12.

[24] D. Reinoso, M. Adrover, M. Pedernera, Green synthesis of nanocrystalline faujasite zeolite, *Ultrasonics sonochemistry* 42 (2018) 303-309.

[25] X. Tu, H.J. Gallon, J.C. Whitehead, Electrical and spectroscopic diagnostics of a single-stage plasma-catalysis system: effect of packing with TiO₂, *Journal of Physics D: Applied Physics* 44(48) (2011) 482003.

[26] H. Kim, A. Ogata, Interaction of nonthermal plasma with catalyst for the air pollution control, *Int. J. Plasma Environ. Sci. Technol* 6(1) (2012) 43-48.

[27] B. Patil, N. Cherkasov, J. Lang, A. Ibadon, V. Hessel, Q. Wang, Low temperature plasma-catalytic NO_x synthesis in a packed DBD reactor: Effect of support materials and supported active metal oxides, *Applied Catalysis B: Environmental* 194 (2016) 123-133.

[28] Y. Wang, W. Yang, S. Xu, S. Zhao, G. Chen, A. Weidenkaff, C. Hardacre, X. Fan, J. Huang, X. Tu, Shielding protection by mesoporous catalysts for improving plasma-catalytic ambient ammonia synthesis, *Journal of the American Chemical Society* 144(27) (2022) 12020-12031.

[29] K.H. Rouwenhorst, H.-H. Kim, L. Lefferts, Vibrationally excited activation of N₂ in plasma-enhanced catalytic ammonia synthesis: a kinetic analysis, *ACS Sustainable Chemistry & Engineering* 7(20) (2019) 17515-17522.

[30] M. Boudam, B. Saoudi, M. Moisan, A. Ricard, Characterization of the flowing afterglows of an N₂-O₂ reduced-pressure discharge: setting the operating conditions to achieve a dominant late afterglow and correlating the NO β UV intensity variation with the N and O atom densities, *Journal of Physics D: Applied Physics* 40(6) (2007) 1694.

[31] P. Paris, M. Aints, F. Valk, T. Plank, A. Haljaste, K. Kozlov, H. Wagner, Intensity ratio of spectral bands of nitrogen as a measure of electric field strength in plasmas, *Journal of Physics D: Applied Physics* 38(21) (2005) 3894.